Ag-Cu-Ni system

Measurements on the Ag-Cu-Ni system were first reported by de Cesaris **[13deC]** who provided a plot of the liquidus surface and some solidus points. The system was studied again by Guertler and Bergmann **[33Gue]**. Siewert and Heine **[77Sie]** studied phase equilibria at 800 °C and 900 °C and the liquidus surface while more recently Luo and Chen **[96Luo]** studied phase equilibria at 700 °C, 795 °C and 860 °C. Calculations were carried out within the framework of COST 531 to explore the agreement between the current database and the limited experimental data for this system. No ternary interactions were found to be necessary.
Experimental data published prior to the COST Action have been added to calculated isothermal sections to demonstrate validity of critically assessed data.

References:

[13deC] de Cesaris, P.: *Gazz. Chim. Ital*., 1913, **25**, 365-79.

[33Gue] Guertler, W., Bergmann, A.: *Z. Metallkde.*, 1933, **25**, 53-57.

[77Sie] Siewert, T.A., Heien, R.W.: *Metall. Trans. A*, 1977, **8A**. 515-518.

[96Luo] Luo, H.-T., Chen, S.-W.: *J. Mater. Sci.*, 1996, **31**, 5059-5067.

There are no ternary invariant reactions in this system.

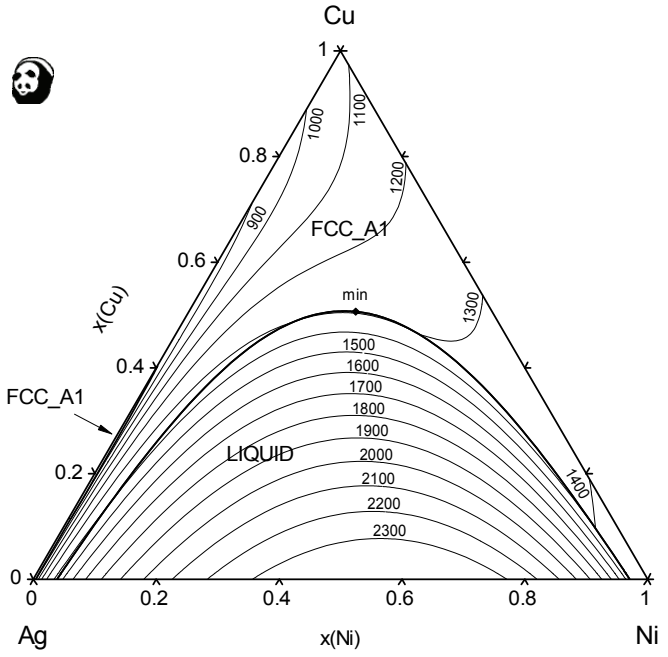

Fig. 92: Liquidus projection of the Ag-Cu-Ni system

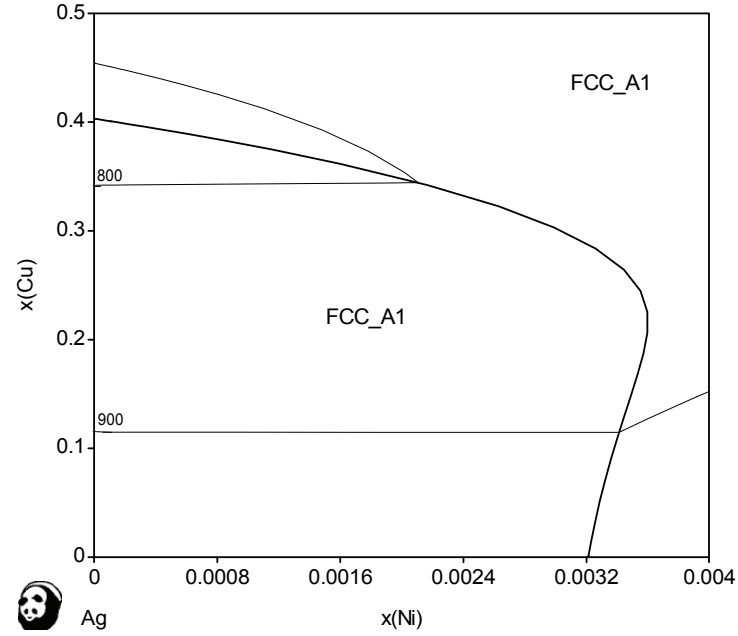

Fig. 93: Liquidus projection for Ag rich corner of the Ag-Cu-Ni system

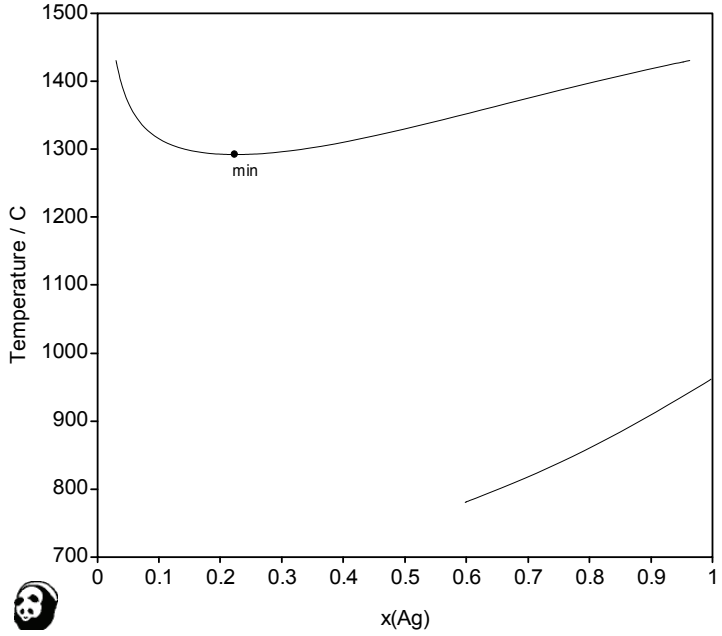

Fig . 94: Liquidus lines in the Ag-Cu-Ni system projected onto the T- x(Ag) plane

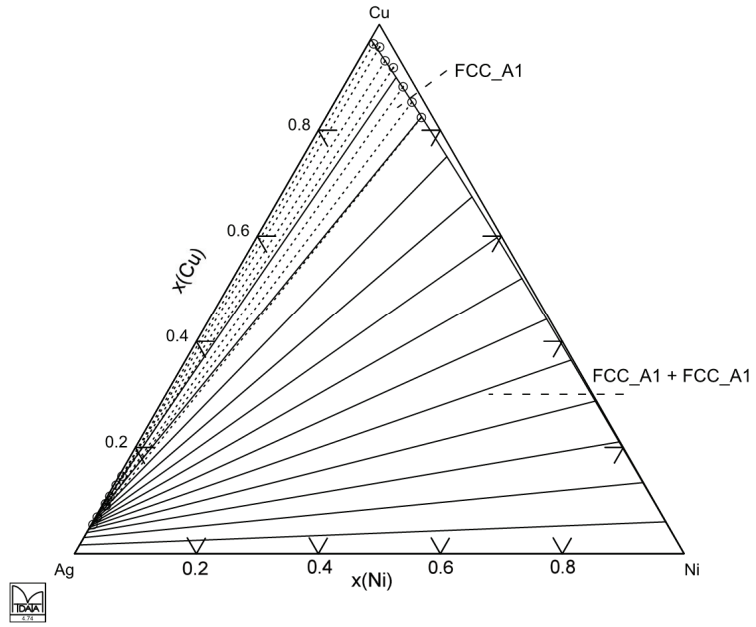

Fig. 95: Isothermal section at 700 °C with experimental data of Luo and Chen **[96Luo]** superimposed

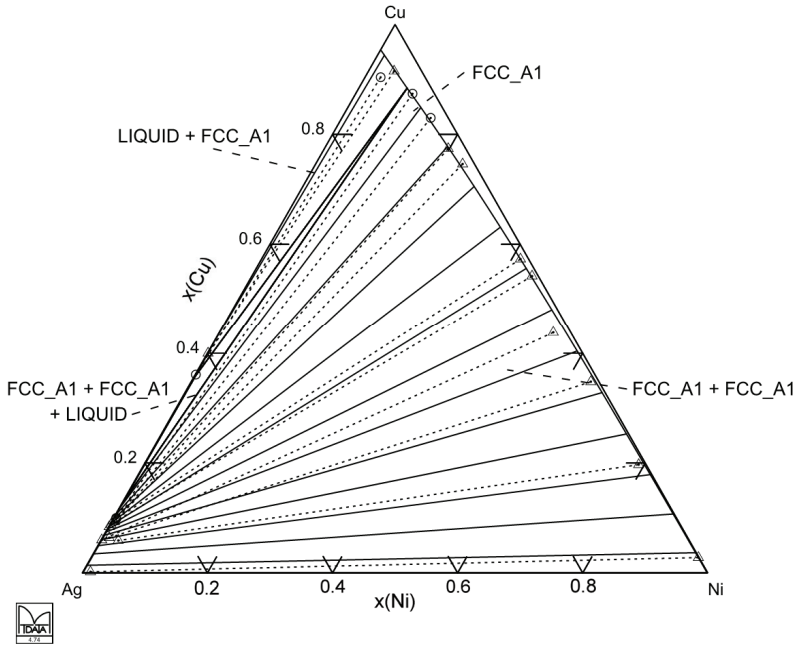

Fig. 96: Isothermal section at 795 °C with experimental data of Luo and Chen **[96Luo]** (❍) and those of Siewert and Heine **[77Sie]** for 800°C (△) superimposed

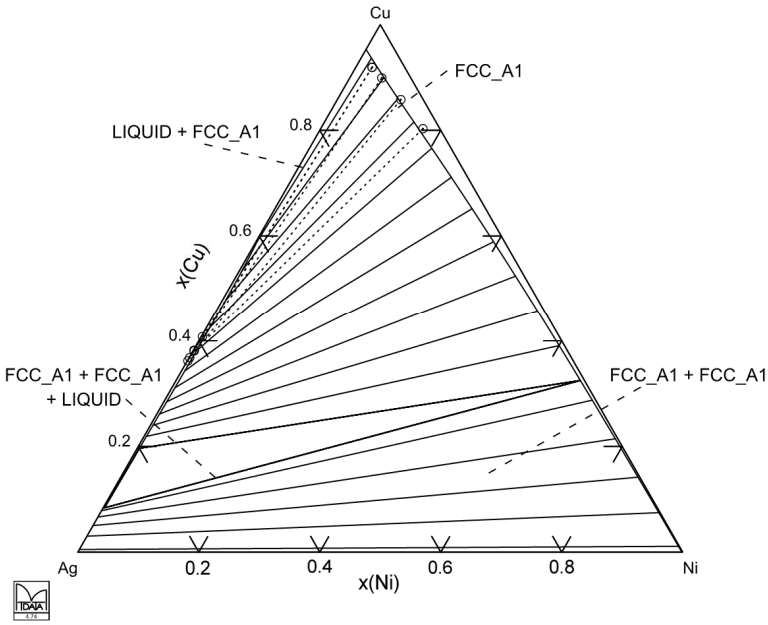

Fig. 97: Isothermal section at 860 °C with experimental data of Luo and Chen **[96Luo]** superimposed

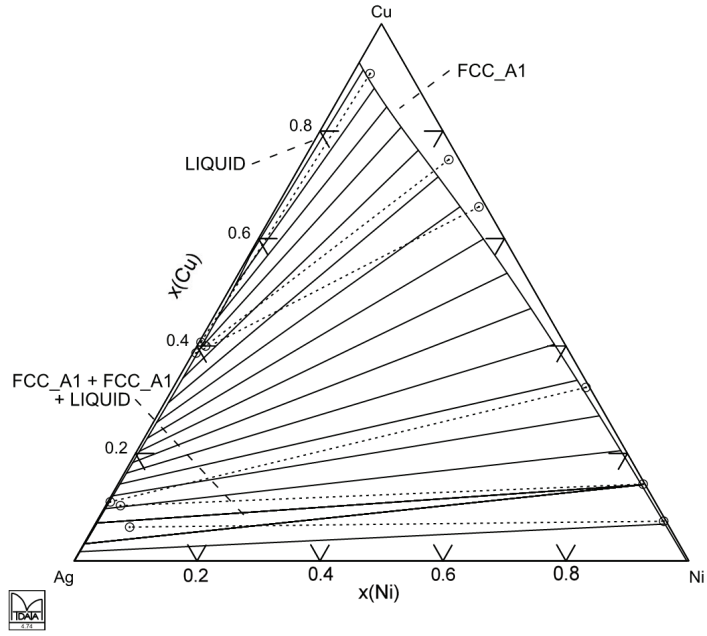

Fig. 98: Isothermal section at 900 °C with experimental data of Siewert and Heine **[77Sie]** superimposed

Ag-Cu-Pb System

The data for this system was accepted from the well established assessment of **[86Hay]** which is in very good agreement with the experimental data. Only one invariant reaction very close to the Pb-rich corner exists in this system. Three FCC_A1 phases with very limited solubilities of other elements are the result of the reaction.

References:

[86Hay] Hayes, F., Lukas, H. L., Effenberg, G., Petzow, G.: *Z. Metallkde.*, 1986, **77**, 749-754.

Table of invariant reactions

T / °C	Reaction type	Phases	Compositions		
			x_{Ag}	x_{Cu}	x_{Pb}
138.5	E1	LIQUID	0.045	0.002	0.953
		FCC_A1#1	0.989	0.004	0.007
		FCC_A1#2	0.001	0.998	0.001
		FCC_A1#3	0.002	0.001	0.997

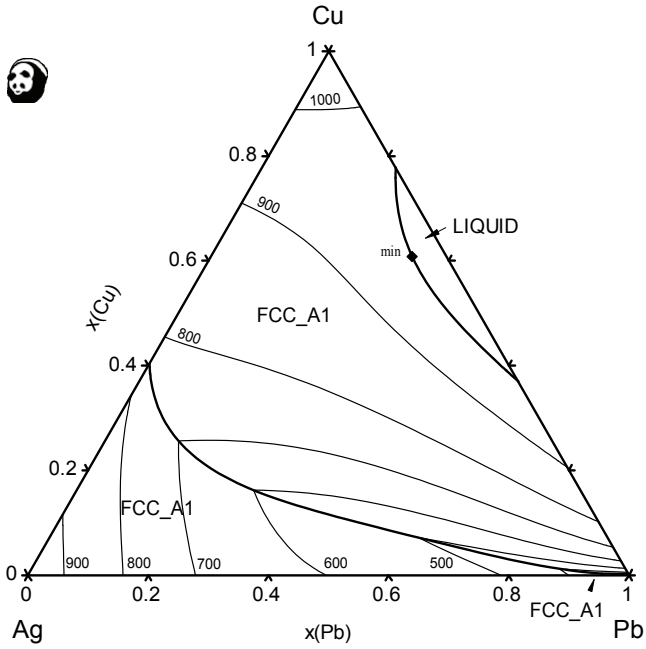

Fig. 99: Liquidus projection of the Ag-Cu-Pb system

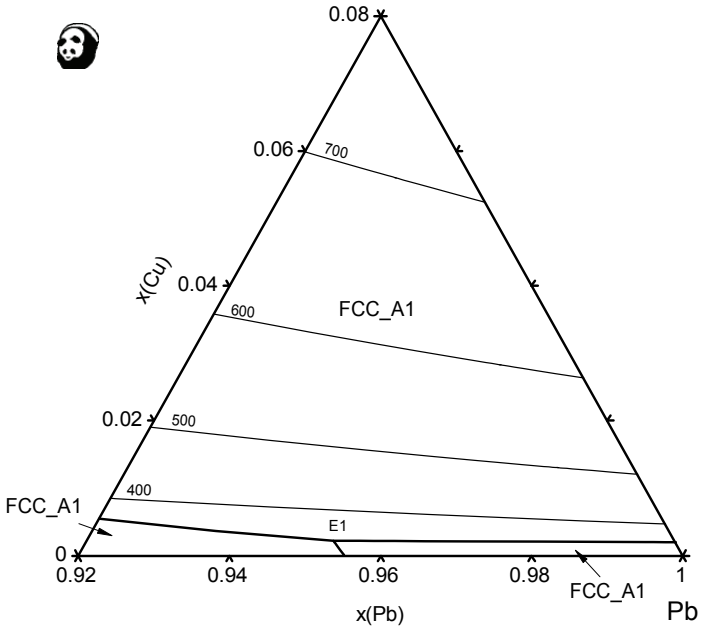

Fig. 100: Pb–rich corner of the liquidus surface of the Ag-Cu-Pb system

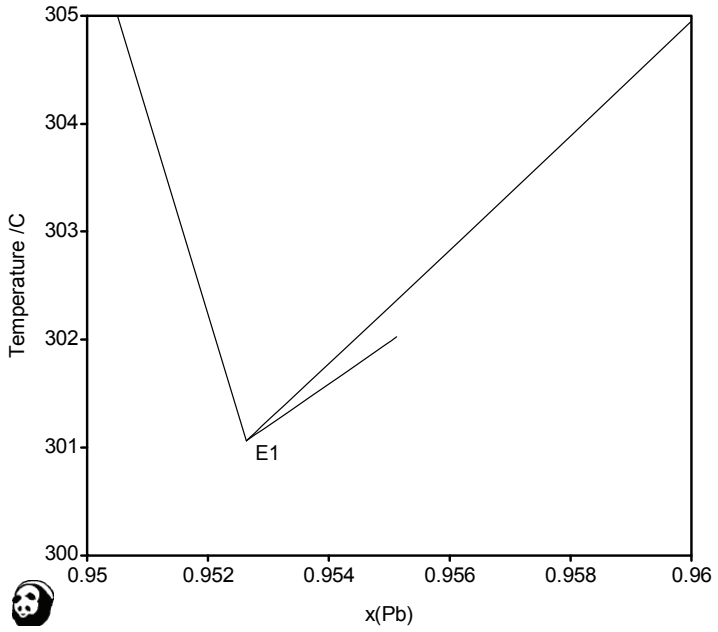

Fig. 101: Liquidus lines in the Ag-Cu-Pb system in the region of the low-temperature invariants projected onto the T- x(Pb) plane

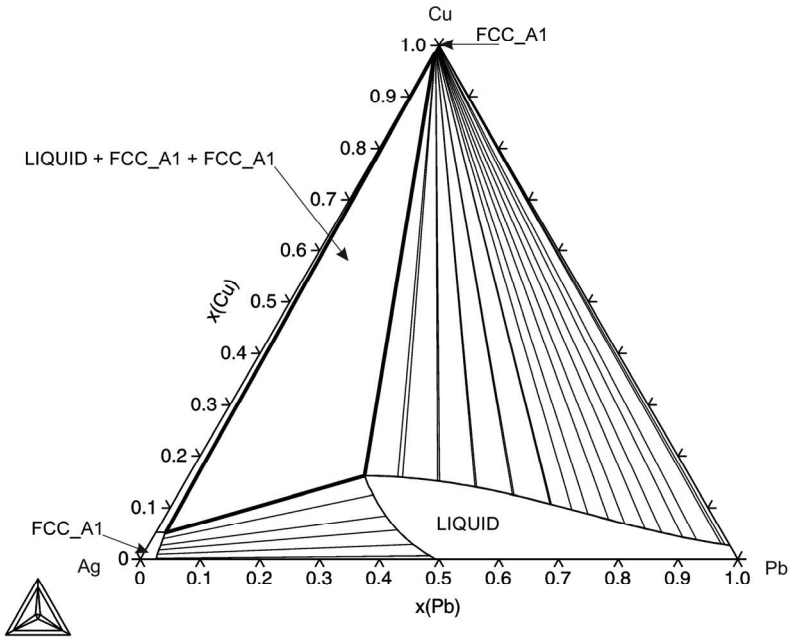

Fig. 102: Isothermal section at 600 °C

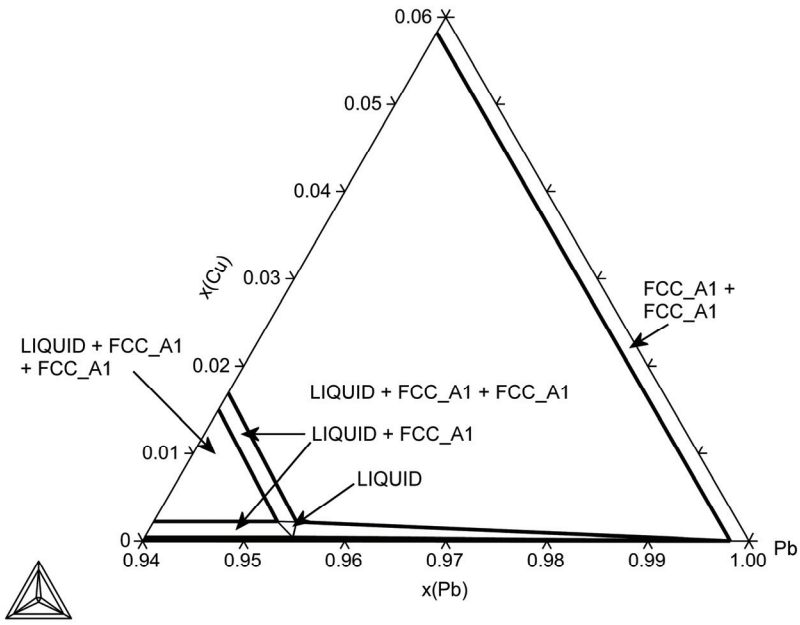

Fig. 103: Pb-rich corner of the isothermal section at 302 °C of the Ag-Cu-Pb system (close to eutectic point)

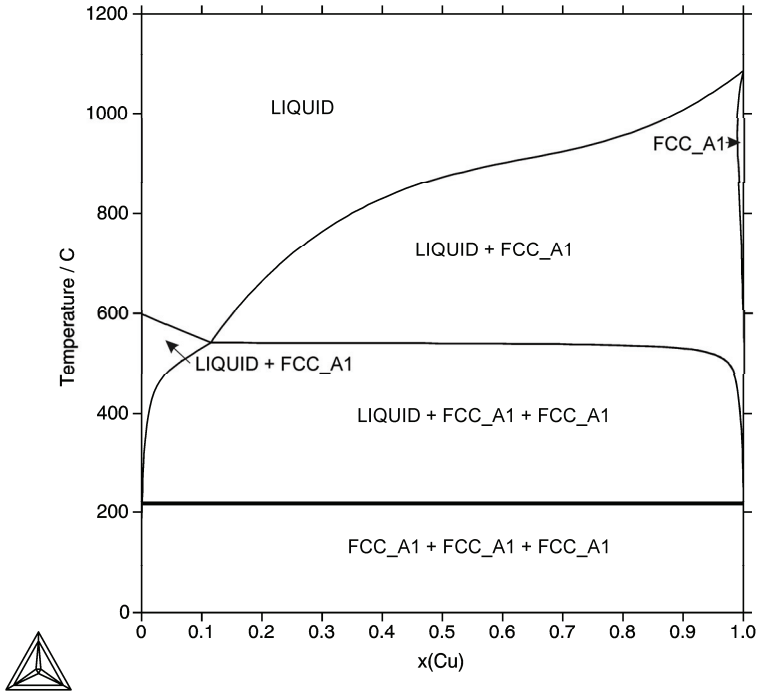

Fig. 104: Isopleth of the Ag-Cu-Pb system with the ratio Ag:Pb of 1:1

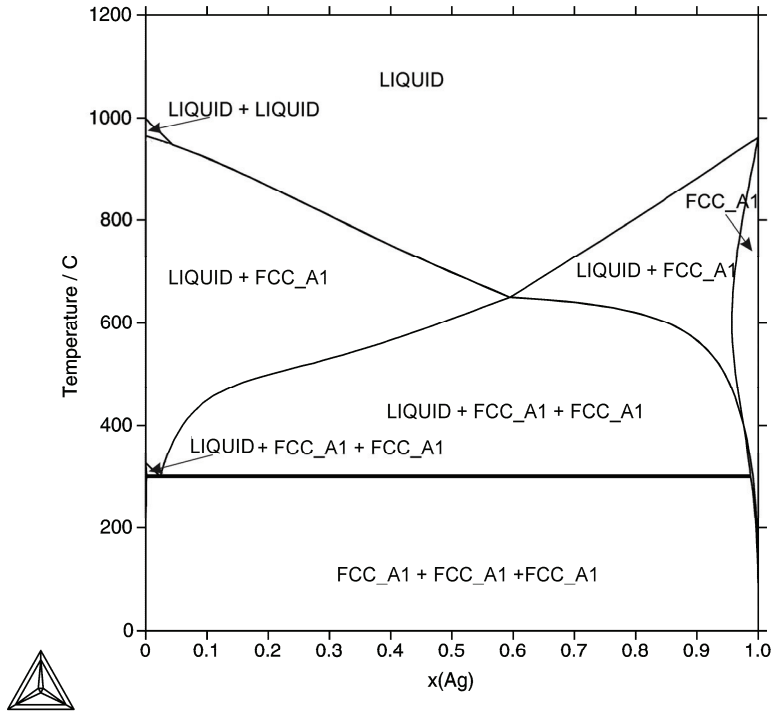

Fig. 105: Isopleth of the Ag-Cu-Pb system with the ratio Cu:Pb of 1:1

Ag-Cu-Sn system

The data for the Ag-Cu-Sn system were taken from an unpublished assessment of Gisby and Dinsdale carried out prior the COST 531 Action. Recent measurements of the enthalpies of mixing and emf in the liquid phase by Flandorfer and Zabdyr respectively undertaken within the COST 531 Action have not been taken into account. The assessment was based on calorimetry data of Shen *et al.* **[69She1, 69She2]**, studies of the solubility of Cu in Ag-Sn liquids by **[99Cha]** and studies of phase equilibria for various isopleths in the ternary system **[59Geb, 81Fed, 82Fed, 94Mil, 00Loo, 00Moo]**.
Because of great importance of this system for the industry, the **Figs. 111-115** are shown in wt. fractions, allowing better orientation in the phase diagram with respect to the most common compositions of industrial alloys.

References:

[59Geb] Gebhardt, R. E. G., Petzow, G.: *Z. Metallkde*, 1959, **50**, 597-605.

[69She1] Shen, S. S.: Ph.D. Thesis, 1969, University of Denver.

[69She2] Shen, S. S., Spencer, P. J., Pool, M. J.: *Trans. AIME*, 1969, **245**, 603-606.

[81Fed] Fedorov, V. N., Osinchev, O. E., Yushkina, E. T.: *Fazovye Ravnovesiya Met. Splavakh*, 1981, 42-49.

[82Fed] Fedorov, V. N., Osinchev, O. E., Yushkina, E. T.: in Phase Diagrams of Metallic Systems, 1982, Ed. Ageev, N. V., Petrova, L. A., **26**, 149-150.

[94Mil] Miller, C. M., Anderson, I. E., Smith, J. F.: *J. Electron. Mat.*, 1994, **23**, 595-601.

[99Cha] Chada, S., Laub, W., Fournelle, R. A., Shangguan, D.: *J. Electron. Mat.*, 1999, **26**, 1194-1202.

[00Loo] Loomans, M. E., Fine, M. E.: *Metall. Mater. Trans. A*, 2000, **31A**, 1155-1162.

[00Moo] Moon, K. W., Boettinger, W. J., Kattner, U. R., Biancaniello, F. S., Handwerker, C. A.: *J. Electron. Mat.*, 2000, **29**, 1122-1136.

Table of invariant reactions

T / °C	Reaction type	Phases	Compositions		
			x_{Ag}	x_{Cu}	x_{Sn}
600.2	U1	LIQUID	0.415	0.422	0.163
		BCC_A2	0.028	0.821	0.151
		FCC_A1	0.896	0.039	0.065
		FCC_A1	0.012	0.914	0.074
560.7	U2	LIQUID	0.436	0.342	0.222
		BCC_A2	0.033	0.769	0.198
		FCC_A1	0.874	0.022	0.104
		CU3SN	0.000	0.750	0.250
552.2	U3	LIQUID	0.450	0.308	0.242
		FCC_A1	0.865	0.019	0.116
		HCP_A3	0.857	0.011	0.132
		CU3SN	0.000	0.750	0.250
441.0	U4	LIQUID	0.383	0.182	0.435
		HCP_A3	0.780	0.002	0.218
		AGSB_ORTHO	0.750	0.000	0.250
		CU3SN	0.000	0.750	0.250
349.5	U5	LIQUID	0.225	0.122	0.653
		CU3SN	0.000	0.750	0.250
		AGSB_ORTHO	0.750	0.000	0.250
		CUIN_ETA	0.000	0.545	0.455
217.5	E1	LIQUID	0.036	0.016	0.948
		BCT_A5	0.001	0.000	0.999
		AGSB_ORTHO	0.750	0.000	0.250
		CUIN_ETA	0.000	0.545	0.455

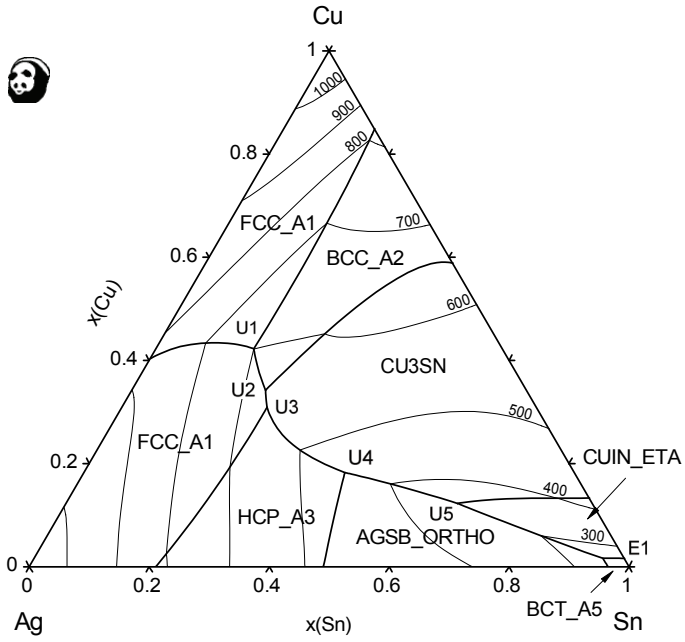

Fig. 106: Liquidus projection of the Ag-Cu-Sn system

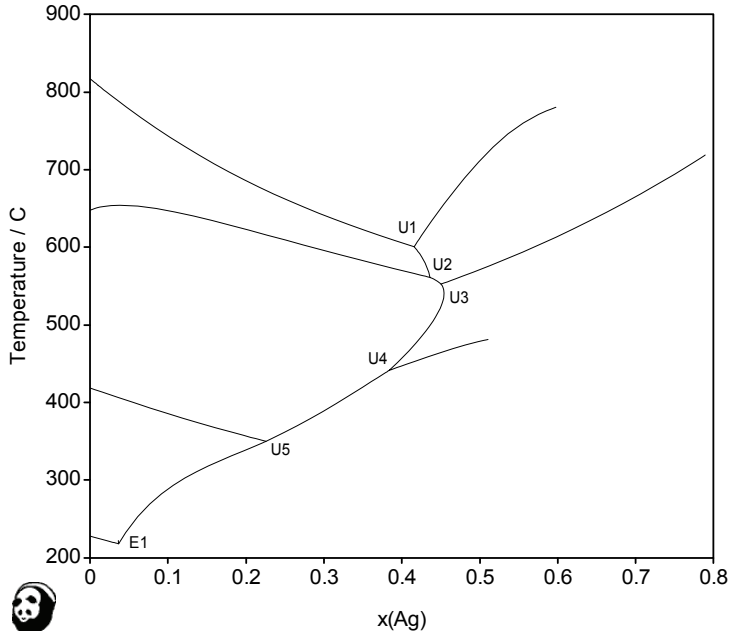

Fig. 107: Liquidus lines in the Ag-Cu-Sn system projected onto the T- x(Ag) plane

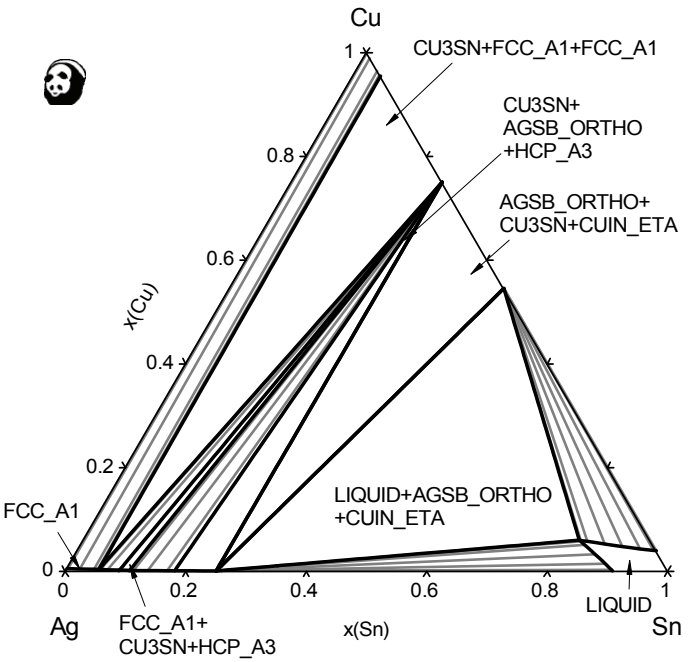

Fig. 108: Isothermal section at 300 °C

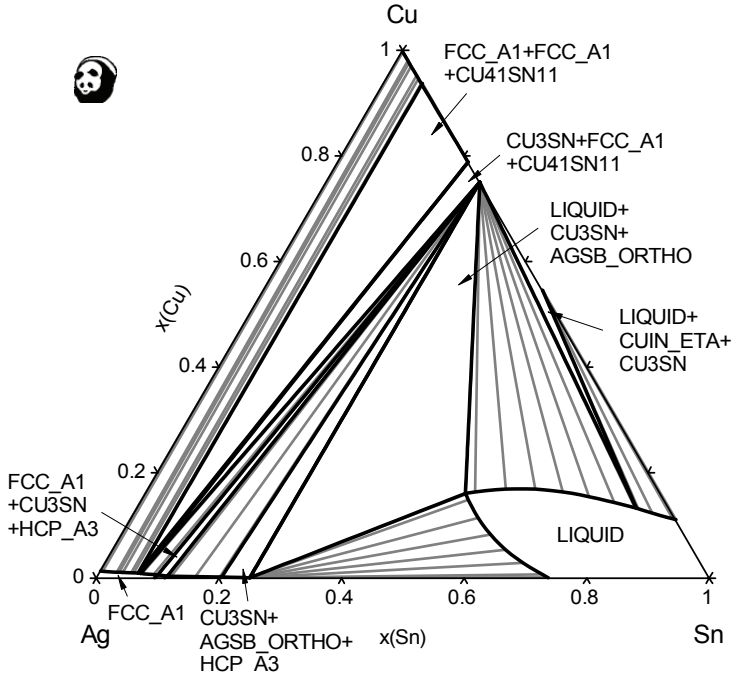

Fig. 109: Isothermal section at 400 °C

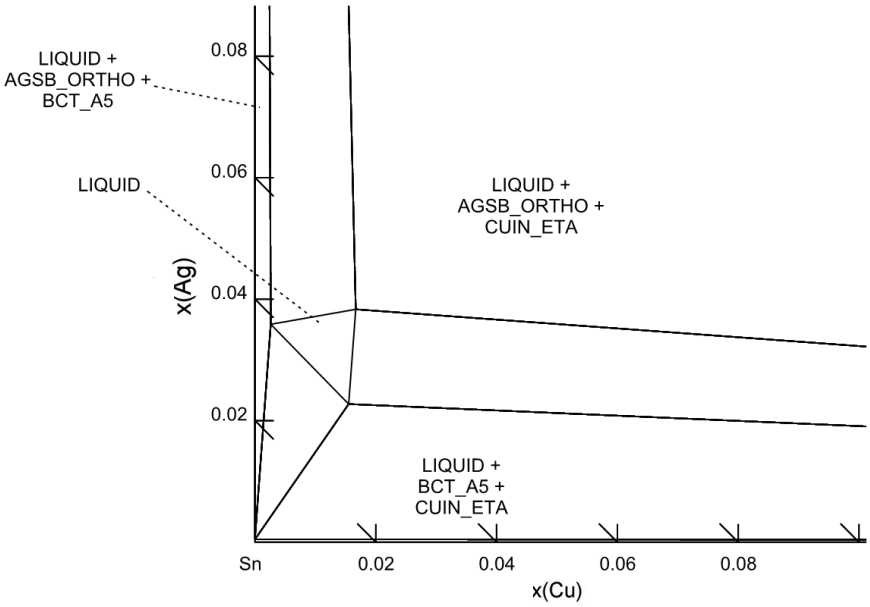

Fig. 110: Isothermal section of Sn rich corner of the Ag-Cu-Sn system at 221 °C

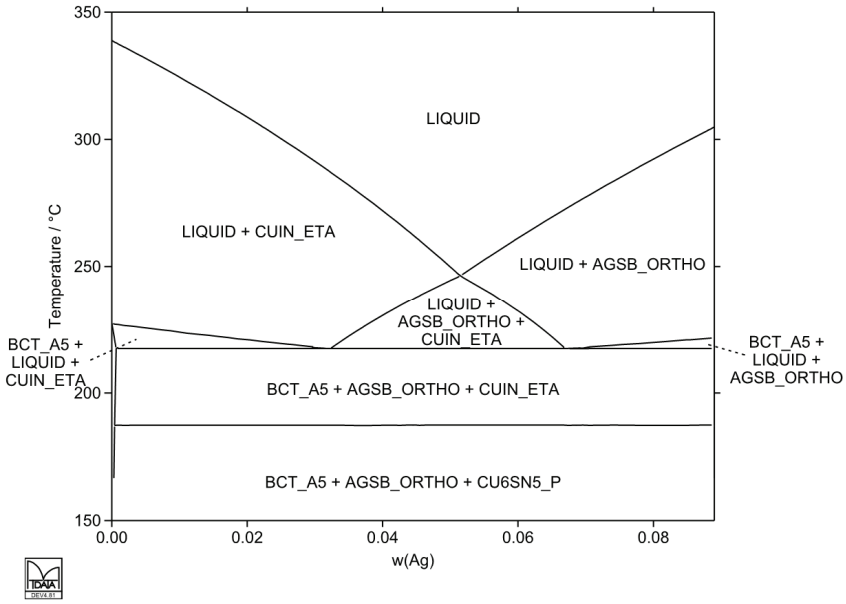

Fig. 111: Isopleth of the Ag-Cu-Sn system from Sn-3.27 wt % Cu to Sn-8.9 wt % Ag

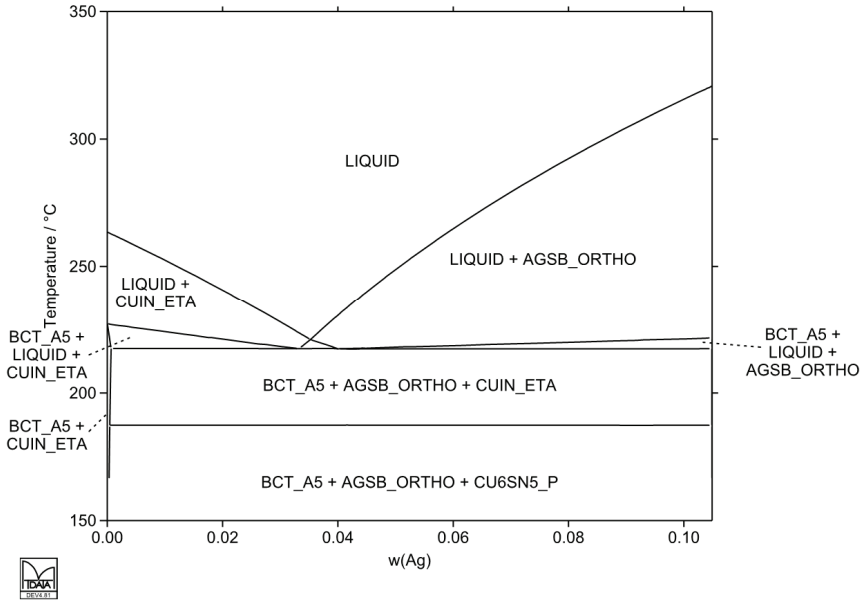

Fig. 112: Isopleth of the Ag-Cu-Sn system from Sn-1.36 wt % Cu to Sn-10.49 wt % Ag

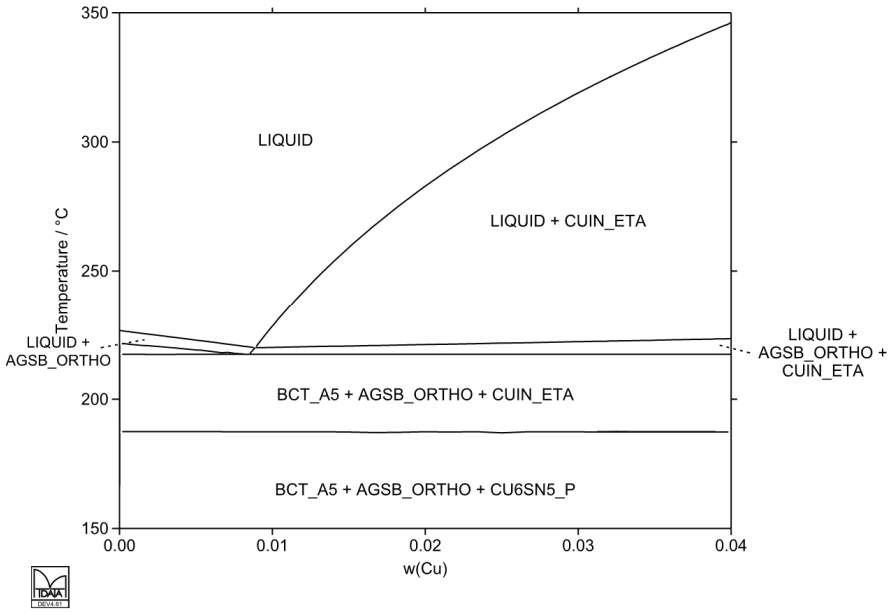

Fig. 113: Isopleth of the Ag-Cu-Sn system from Sn-3.5 wt % Ag to Sn-3.37% wt Ag – 4 wt % Cu

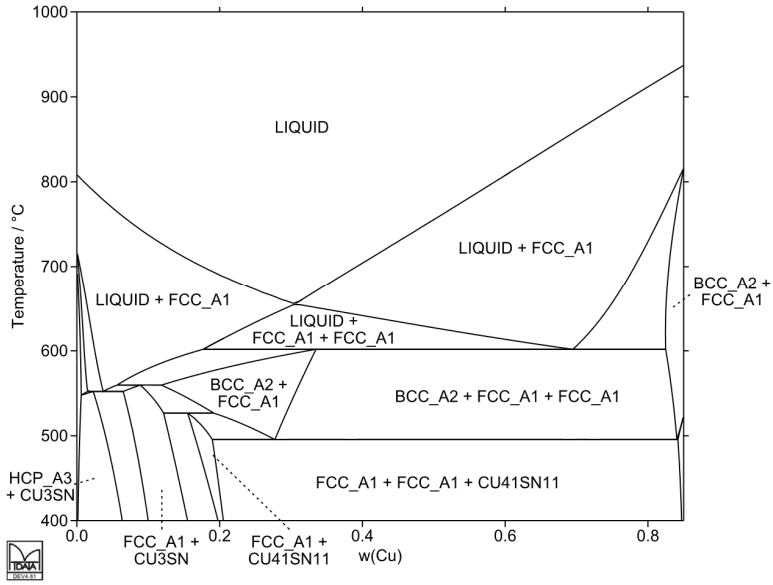

Fig. 114: Isopleth of the Ag-Cu-Sn system for 15 wt % Sn

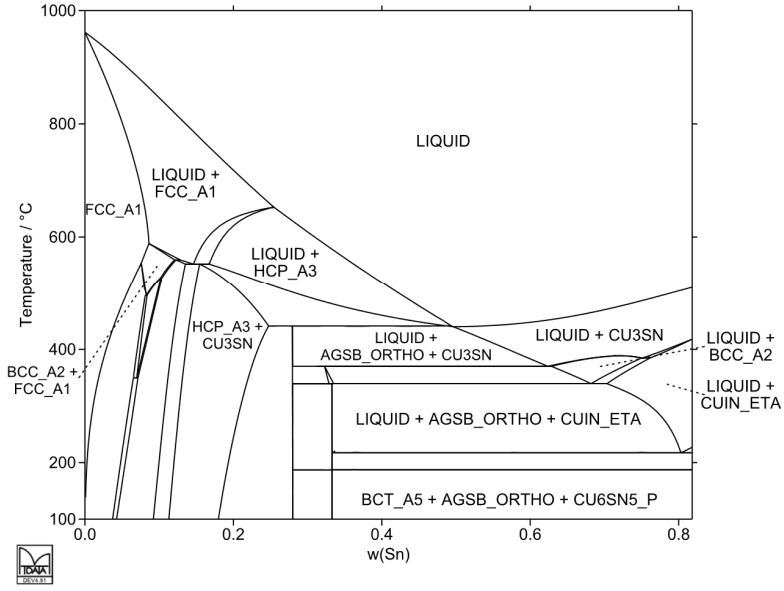

Fig. 115: Isopleth of the Ag-Cu-Sn system from pure Ag to Sn-18.18 wt %Cu

Ag-In-Sn System

The critically assessed data of Liu *et al.* **[02Liu]** were adopted and when used with the COST 531 binary data give very good agreement with experimental information. The liquidus surface is very complex close to the In-Sn binary system and the side projection of the liquidus lines is very useful to indicate the position of particular invariant reactions.

References:

[02Liu] Liu, X., Inohana, Y., Takaku, Y., Ohnuma, I., Kainuma, R., Ishida, K., Moser, Z., Gasior, W., Pstrus, J.: *J. Electron. Mater.,* 2002, **31**, 1139-1151.

Table of invariant reactions

T / °C	Reaction type	Phases	Compositions		
			x_{Ag}	x_{In}	x_{Sn}
674.2	P1	LIQUID	0.699	0.292	0.009
		FCC_A1	0.804	0.195	0.001
		BCC_A2	0.751	0.248	0.001
		HCP_A3	0.759	0.237	0.004
213.6	U1	LIQUID	0.042	0.034	0.924
		AGSB_ORTHO	0.750	0.000	0.250
		HCP_A3	0.715	0.132	0.153
		BCT_A5	0.001	0.011	0.988
207.4	U2	LIQUID	0.037	0.077	0.886
		BCT_A5	0.001	0.025	0.974
		INSN_GAMMA	0.000	0.043	0.957
		HCP_A3	0.700	0.203	0.097
167.7	U3	LIQUID	0.0022	0.325	0.653
		HCP_A3	0.668	0.299	0.033
		CUIN_GAMMA	0.675	0.325	0.000
		INSN_GAMMA	0.000	0.153	0.846

133.7	U4	LIQUID	0.014	0.846	0.140
		TETRAG_A6	0.000	0.877	0.123
		TET_ALPHA1	0.000	0.868	0.132
		AGIN2	0.330	0.670	0.000
118.8	U5	LIQUID	0.010	0.602	0.388
		AGIN2	0.330	0.670	0.000
		TET_ALPHA1	0.000	0.631	0.369
		CUIN_GAMMA	0.672	0.328	0.000
113.5	E1	LIQUID	0.009	0.529	0.463
		TET_ALPHA1	0.000	0.562	0.438
		CUIN_GAMMA	0.672	0.328	0.000
		INSN_GAMMA	0.000	0.228	0.772

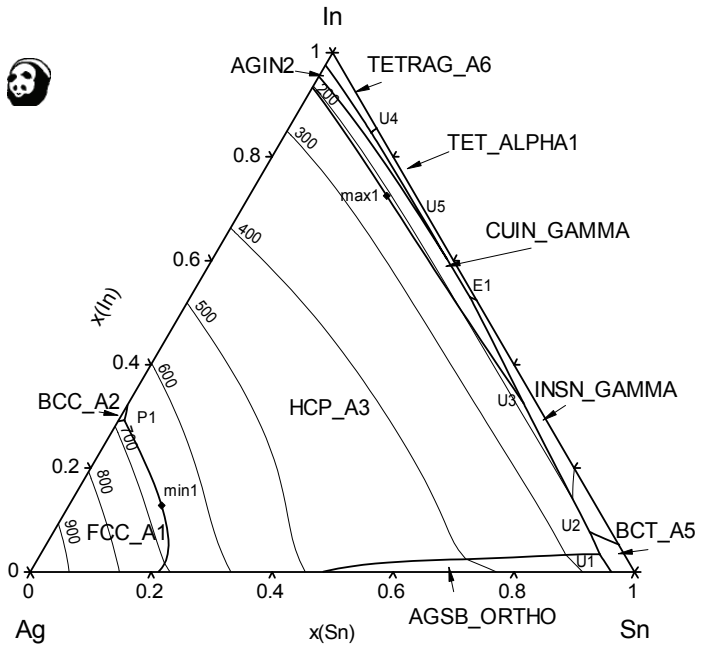

Fig. 116: Liquidus surface of the Ag-In-Sn system

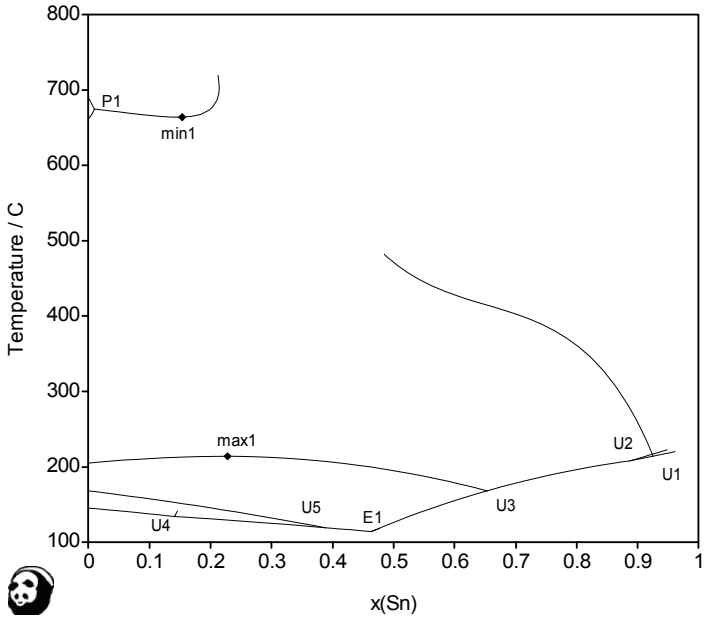

Fig. 117: Liquidus lines in the Ag-In-Sn system projected onto the T- x(Sn) plane

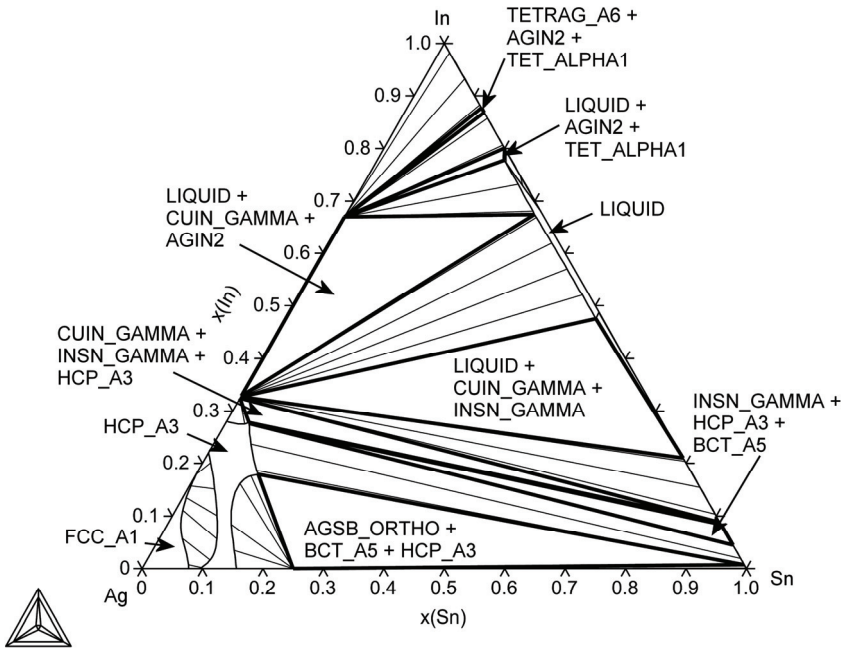

Fig. 118: Isothermal section at 130 °C

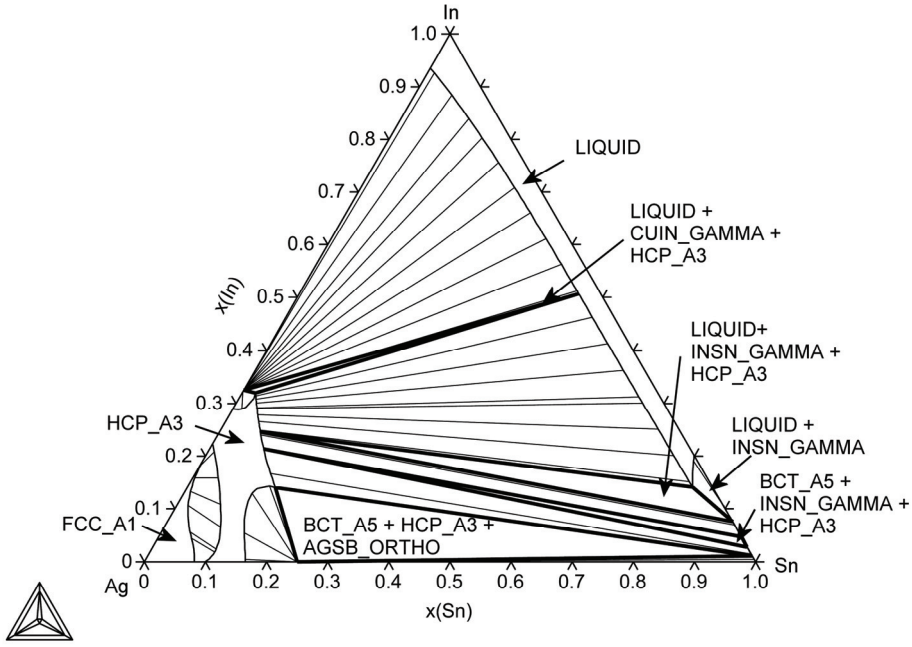

Fig. 119: Isothermal section at 200 °C

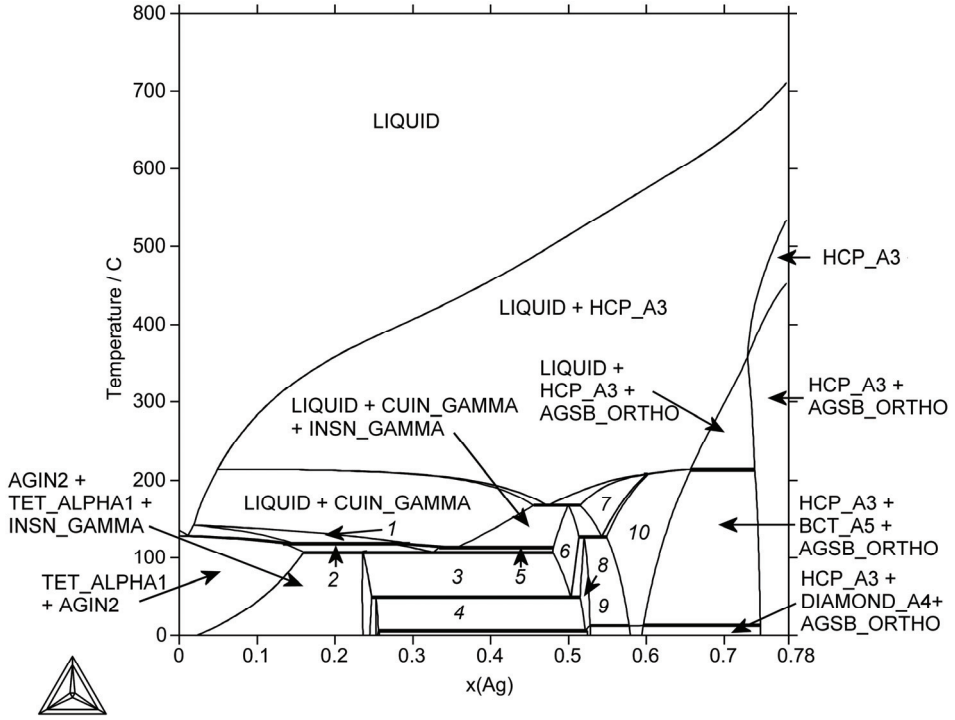

Fig. 120: Isopleth of the Ag-In-Sn system for 22 at% Sn

Legend:

1 – LIQUID + AGIN2 + CUIN_GAMMA
2 – AGIN2 + CUIN_GAMMA + TET_ALPHA1
3 – AGIN2 + CUIN_GAMMA + INSN_GAMMA
4 – BCT_A5 + CUIN_GAMMA + INSN_GAMMA
5 – INSN_GAMMA + CUIN_GAMMA + TET_ALPHA1
6 – INSN_GAMMA + CUIN_GAMMA
7 – HCP_A3 + INSN_GAMMA
8 – BCT_A5 + CUIN_GAMMA
9 – BCT_A5 + CUIN_GAMMA + HCP_A3
10 – BCT_A5 + HCP_A3

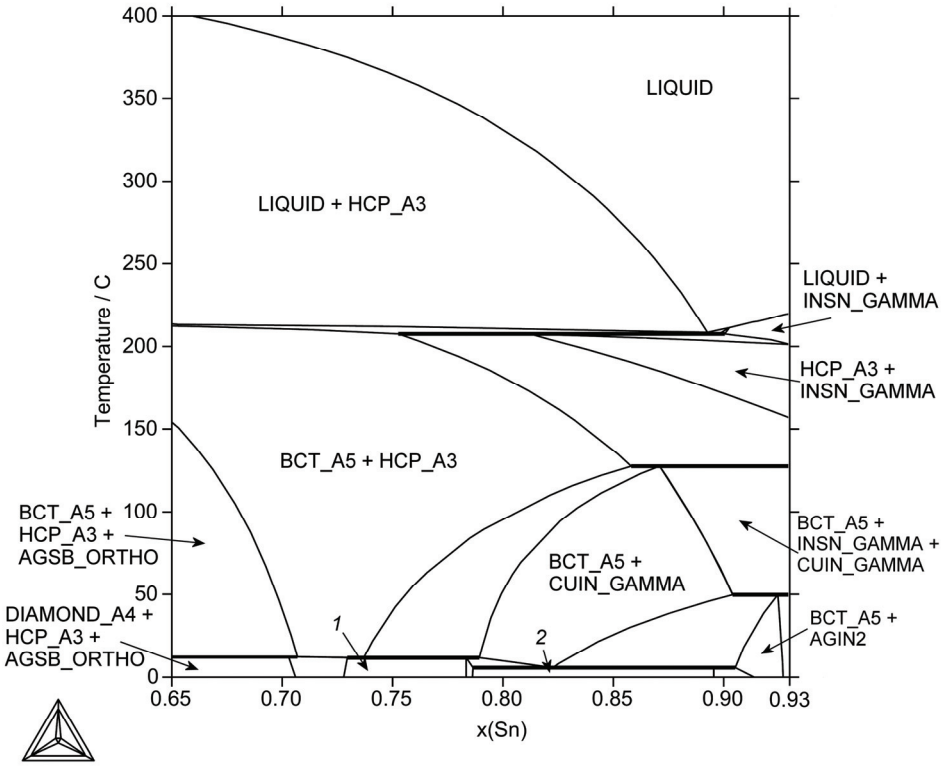

Fig. 121: Part of the isopleth of the Ag-In-Sn system for 7 at% In in the Sn-rich corner (close to the invariant point U3)

Legend:

1 – CUIN_GAMMA + HCP_A3 + DIAMOND_A4
2 – CUIN_GAMMA + AGIN2 + DIAMOND_A4

Ag-Ni-Sn System

There are very few published experimental data for this system. More recently extensive studies of the phase diagram have been undertaken by Schmetterer **[07Sch]**. Ternary interaction data for the liquid phase have been introduced in the scope of COST 531 Action and these give reasonable agreement with experimental properties measured by **[07Sch].**

The liquidus projection of this system is very complex owing to the properties of the binary Ag-Ni system. It is unusual as it exhibits both liquid and solid phase immiscibility. This leads to the presence of two monotectic reactions in the binary phase diagram, and these have a great effect on the equilibria in the ternary Ag-Ni-Sn system. The ternary phase diagram is dominated by a large region of liquid immiscibility that extends from the binary Ag-Ni system. Associated with this miscibility gap are two decomposition reactions, E1 and E2 where the Ni-rich liquid decomposes to give a liquid rich in Ag along with two solid phases. The compositions of the two liquids taking part in these reactions are denoted as E1', E1'', and E2' and E2'', respectively. To add further complication, there are 4 maxima associated with this miscibility gap, and these are linked together in pairs. The maxima e1' and e1'' are maxima on liquidus lines that are tied together in the same monovariant reaction. The maxima e2' and e2'' are linked in the same way. A 4th monovariant is present as a minimum, again associated with the liquid miscibility gap in the ternary system. This minimum represents the point where the critical point of the miscibility gap meets the monovariant line. Interestingly, U4 represents a reaction associated with the reprecipitation of the liquid phase. Owing to the complexity of the liquidus surface of this system, it is necessary to depict the equilibria in a number of diagrams. **Fig. 122** shows the complete liquidus surface and the full extent of the liquid miscibility gap can be seen. Many of the invariant equilibria are not shown here for the sake of clarity, but **Fig. 123** shows the Ag-rich corner of the diagram with Cartesian axes. But possibly the best way to see the invariant reactions, and in particular the maxima and minimum is by the T-x(Sn) plots shown in **Figs. 124** and **125**, where the former shows the liquidus lines for the full system and the latter for the Ag-rich region of the diagram.

References:

[07Sch] Schmetterer, C.: "Interactions of Sn-containing solders with Ni(P) substrates - phase equilibria and thermodynamics", thesis, University of Vienna, 2007.

Table of invariant reactions

T / °C	Reaction type	Phases	Compositions		
			x_{Ag}	x_{Ni}	x_{Sn}
1129.1	e1	LIQUID(e1' max)	0.188	0.473	0.339
		LIQUID(e1"max)	0.752	0.044	0.203
		NI3SN2	0.000	0.615	0.385
1120.0	e2	LIQUID(e2' max)	0.073	0.681	0.246
		LIQUID(e2"max)	0.889	0.018	0.093
		BCC_A2	0.003	0.744	0.253
1106.2	E1	LIQUID (E1')	0.010	0.614	0.286
		BCC_A2	0.002	0.736	0.263
		LIQUID (E1")	0.846	0.023	0.132
		NI3SN2	0.000	0.626	0.374
1098.1	E2	LIQUID (E2')	0.040	0.775	0.185
		FCC_A1	0.003	0.873	0.123
		BCC_A2	0.003	0.758	0.239
		LIQUID (E2")	0.942	0.012	0.047
1089.9	min1	LIQUID#1	0.482	0.159	0.359
		LIQUID#2	0.482	0.159	0.359
		NI3SN2	0.000	.601	.399
942.2	U1	LIQUID	0.975	0.003	0.022
		FCC_A1	0.002	0.907	0.091
		BCC_A2	0.002	0.759	0.239
		FCC_A1	0.990	0.002	0.008
927.8	U2	FCC_A1	0.984	0.002	0.014
		BCC_A2	0.001	0.749	0.250
		LIQUID	0.960	0.003	0.037
		NI3SN_LT	0.000	0.750	0.250

886.2	U3	LIQUID	0.917	0.003	0.080
		BCC_A2	0.001	0.731	0.268
		NI3SN_LT	0.000	0.750	0.250
		NI3SN2	0.000	0.625	0.375
881.3	U4	LIQUID	0.917	0.003	0.080
		NI3SN_LT	0.000	0.750	0.250
		NI3SN2	0.000	0.625	0.375
		FCC_A1	0.963	0.001	0.036
718.4	U5	LIQUID	0.786	0.001	0.213
		FCC_A1	0.885	0.000	0.115
		NI3SN2	0.000	0.588	0.412
		HCP_A3	0.869	0.000	0.131
573.9	U6	LIQUID	0.637	0.002	0.361
		NI3SN2	0.000	0.569	0.431
		NI3SN4	0.000	0.445	0.555
		HCP_A3	0.797	0.000	0.203
481.5	U7	LIQUID	0.506	0.003	0.491
		HCP_A3	0.761	0.000	0.239
		NI3SN4	0.000	0.437	0.563
		AGSB_ORTHO	0.750	0.000	0.250
219.2	E3	LIQUID	0.040	0.002	0.958
		NI3SN4	0.000	0.425	0.575
		AGSB_ORTHO	0.750	0.000	0.250
		BCT_A5	0.001	0.000	0.999

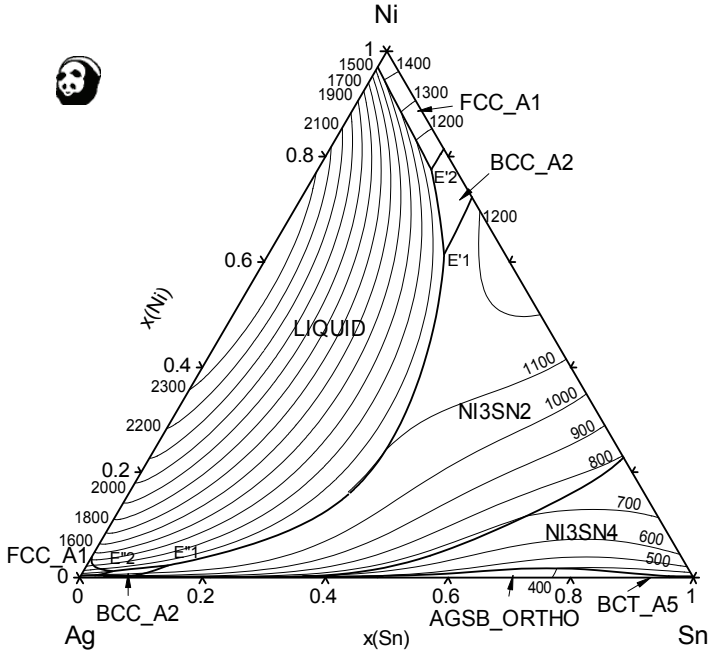

Fig. 122: Liquidus surface of the Ag-Ni-Sn system

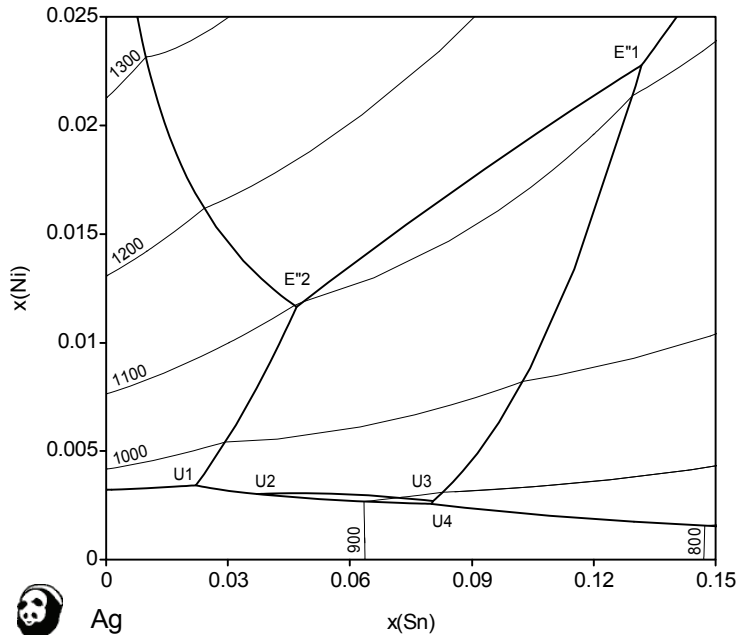

Fig. 123: Liquidus projection of the Ag-Ni-Sn system in the Ag-rich corner

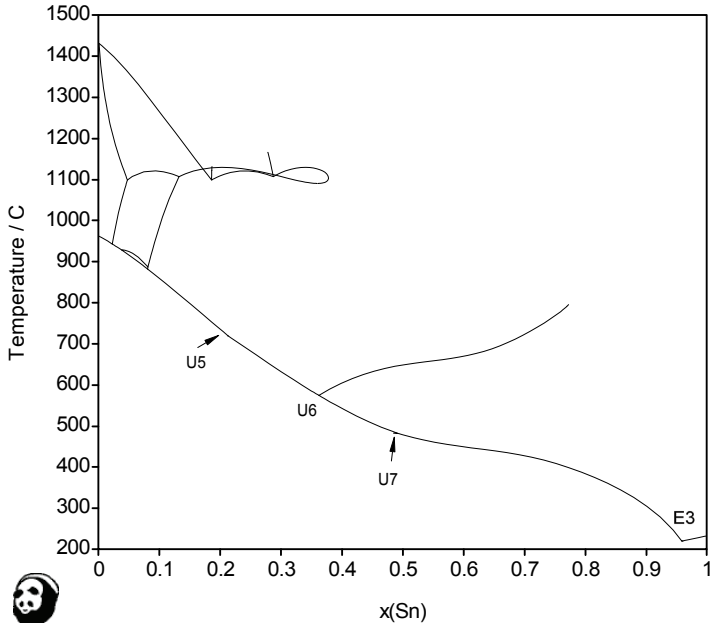

Fig. 124: Liquidus lines in the Ag-Ni-Sn system projected onto the T- x(Sn) plane

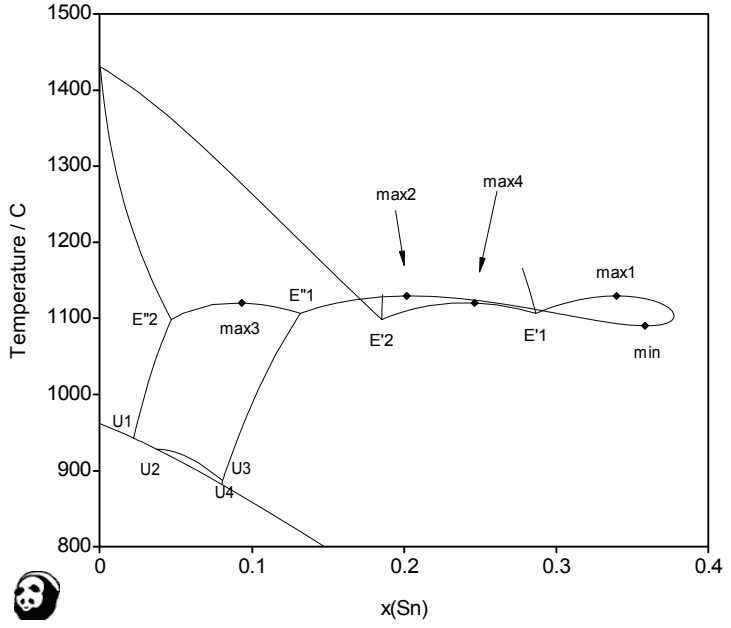

Fig. 125: Liquidus lines in the Ag-Ni-Sn system in the region of the high-temperature invariants projected onto the T- x(Sn) plane

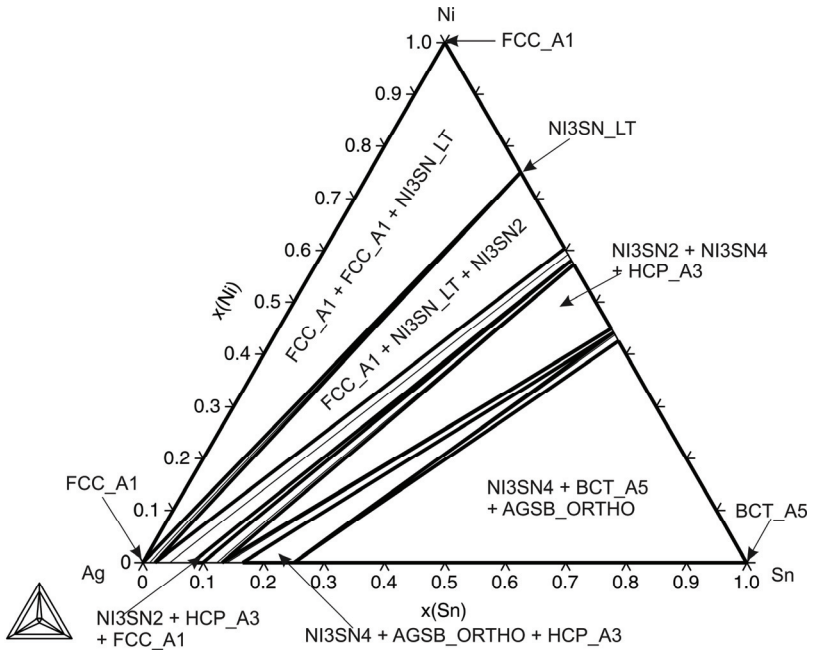

Fig. 126: Isothermal section at 200 °C

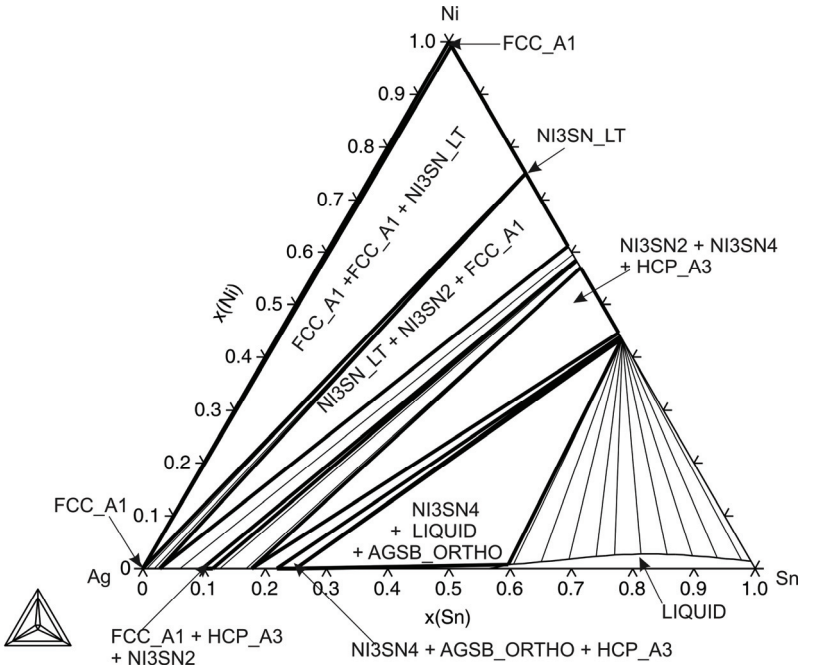

Fig. 127: Isothermal section at 450 °C

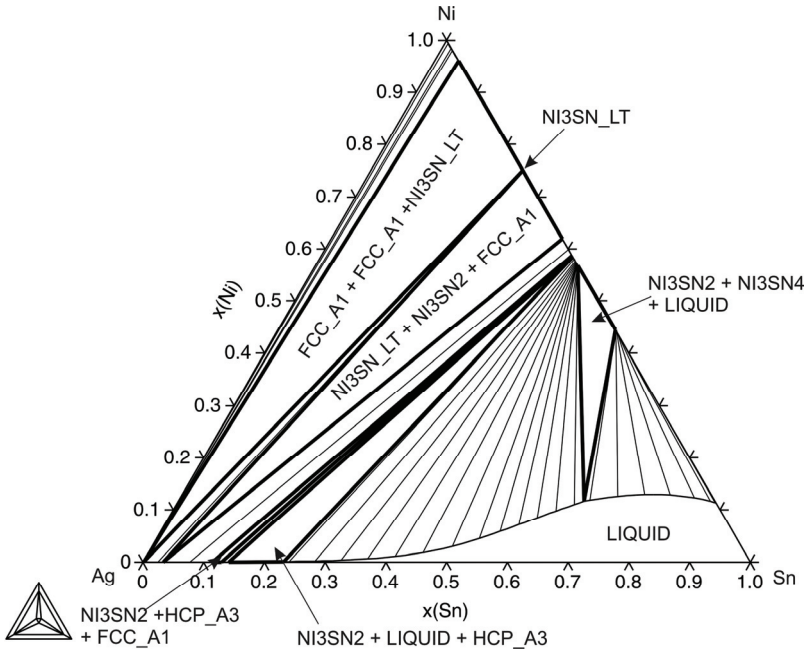

Fig. 128: Isothermal section at 700 °C

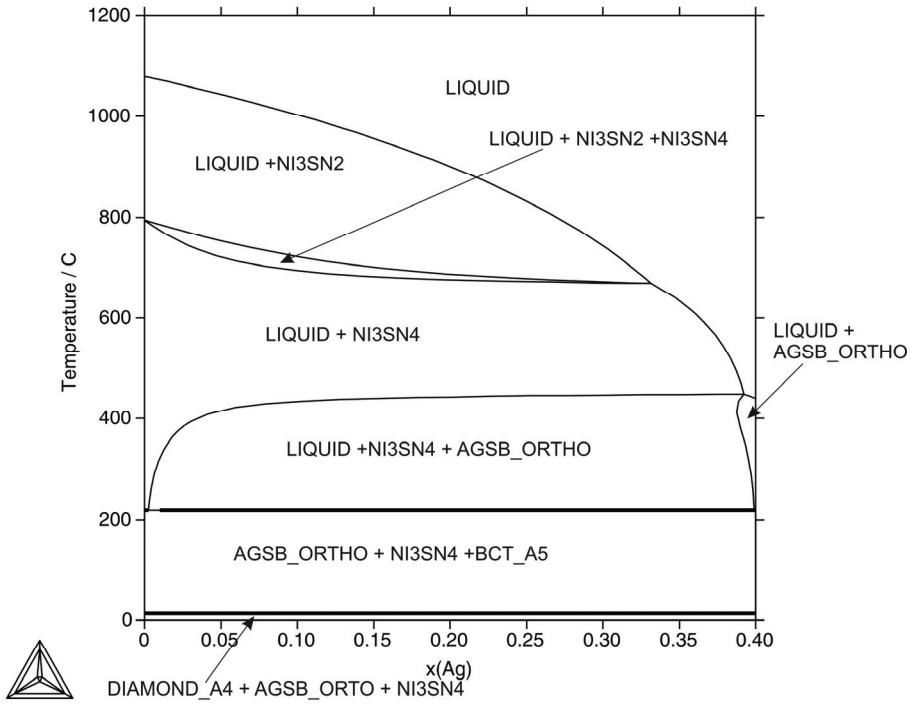

Fig. 129: Isopleth of the Ag-Ni-Sn system for 60 at% Sn

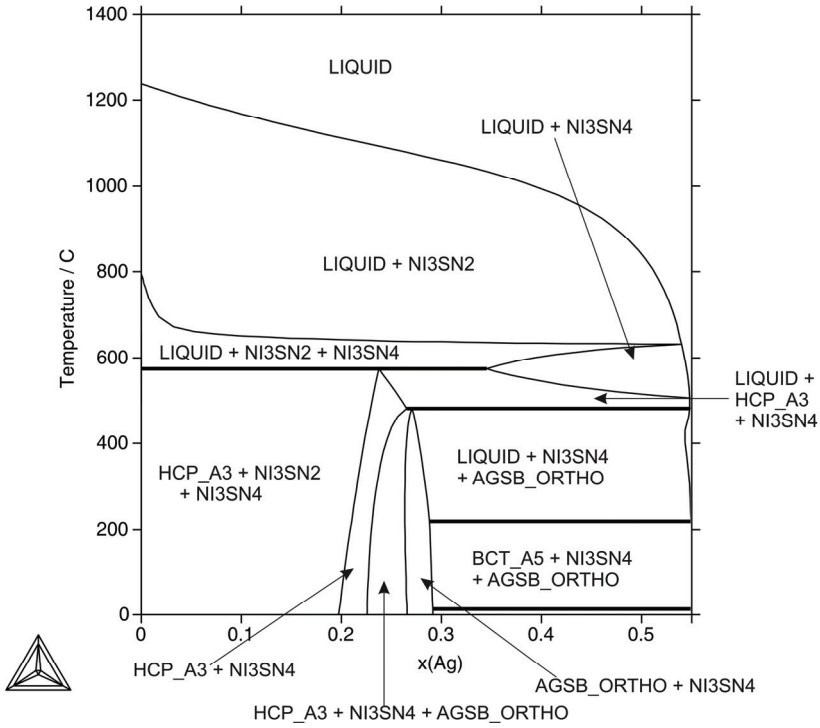

Fig. 130: Isopleth of the Ag-Ni-Sn system for 45 at% Sn

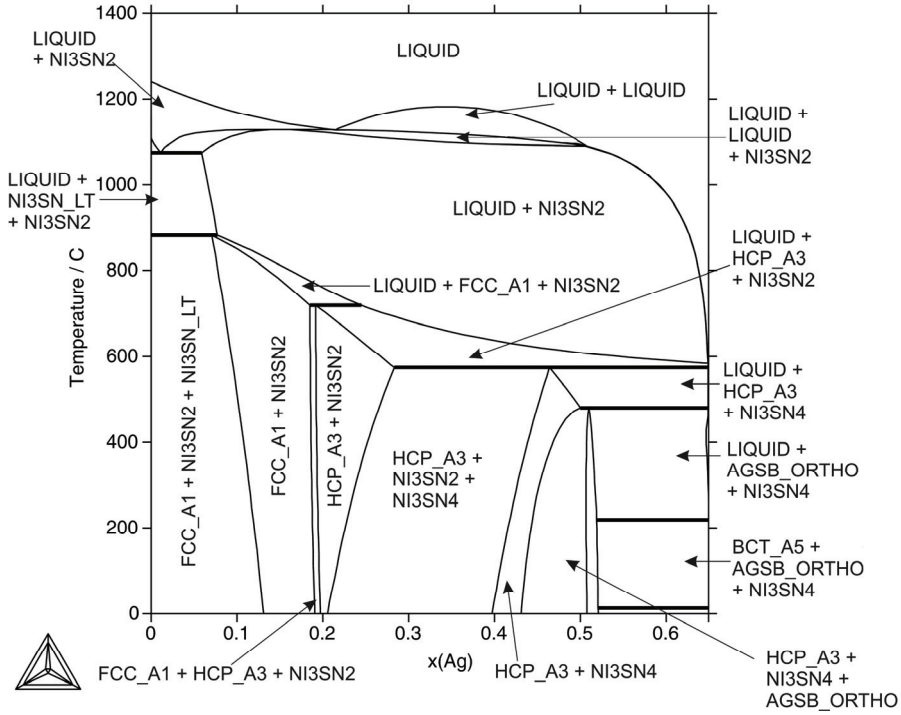

Fig. 131: Isopleth of the Ag-Ni-Sn system for 35 at% Sn

Au-Bi-Sb System

Data from the critical assessment of **[07Wan]** were adopted after checking for consistency with the unary and binary data used in the scope of COST 531 Action. Good agreement was found in comparison with experimental data published in **[07Wan]**.

References:

[07Wan] Wang, J., Meng, F. G., Liu, H. S., Liu, L. B., Jin, Z. P.: *J. Electron Mater.*, 2007, **36**, 568-577.

Table of invariant reactions

T / °C	Reaction type	Phases	Compositions		
			x_{Au}	x_{Bi}	x_{Sb}
296.0	U1	LIQUID	0.422	0.385	0.193
		FCC_A1	0.998	0.000	0.002
		AU2BI_C15	0.667	0.333	0.000
		AU2SB	0.333	0.061	0.606
239.2	E1	LIQUID	0.178	0.774	0.048
		AU2BI_C15	0.667	0.333	0.000
		AU2SB	0.333	0.082	0.585
		RHOMBO_A7	0.000	0.948	0.052

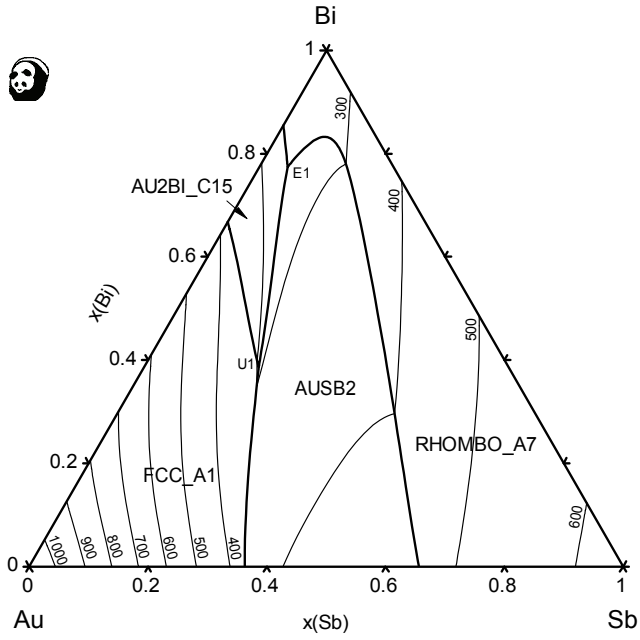

Fig. 132: Liquidus projection for the Au-Bi-Sb system

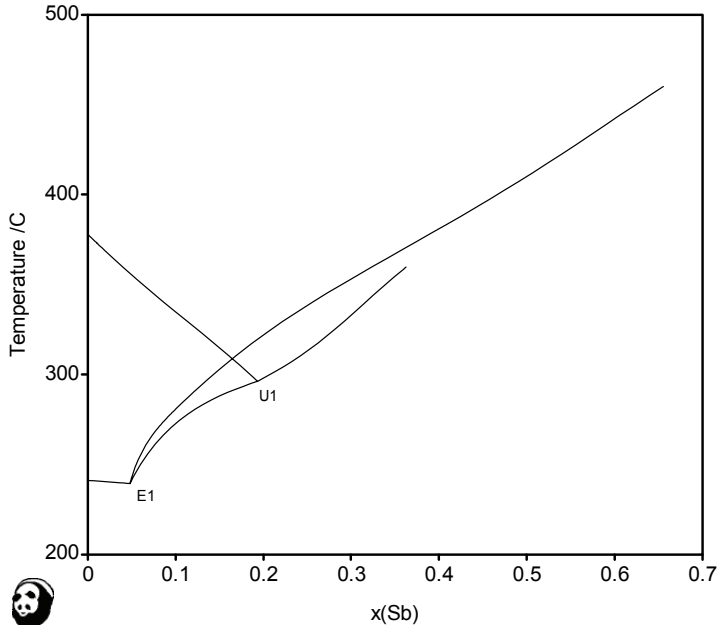

Fig. 133: Liquidus lines in the Au-Bi-Sb system in the region of the low-temperature invariants projected onto the T- x(Sb) plane

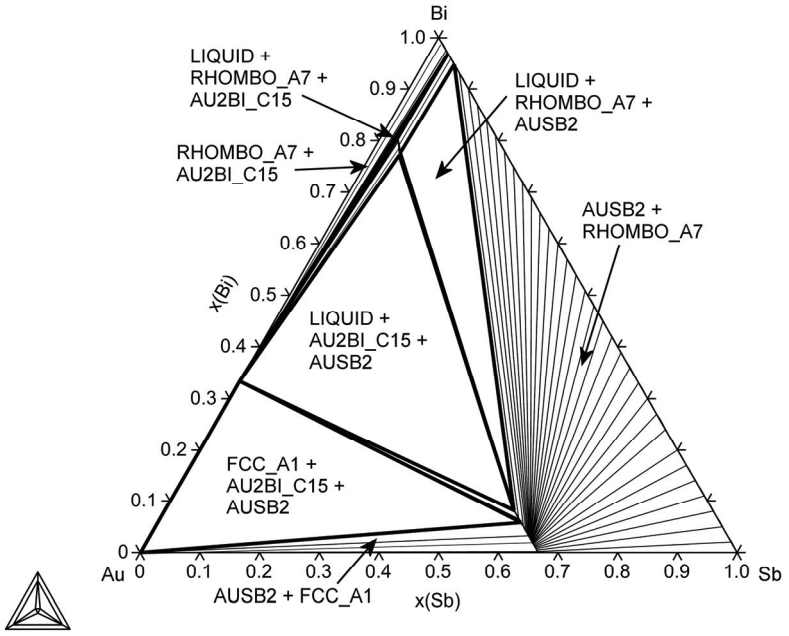

Fig. 134: Isothermal section at 240 °C near the eutectic temperature

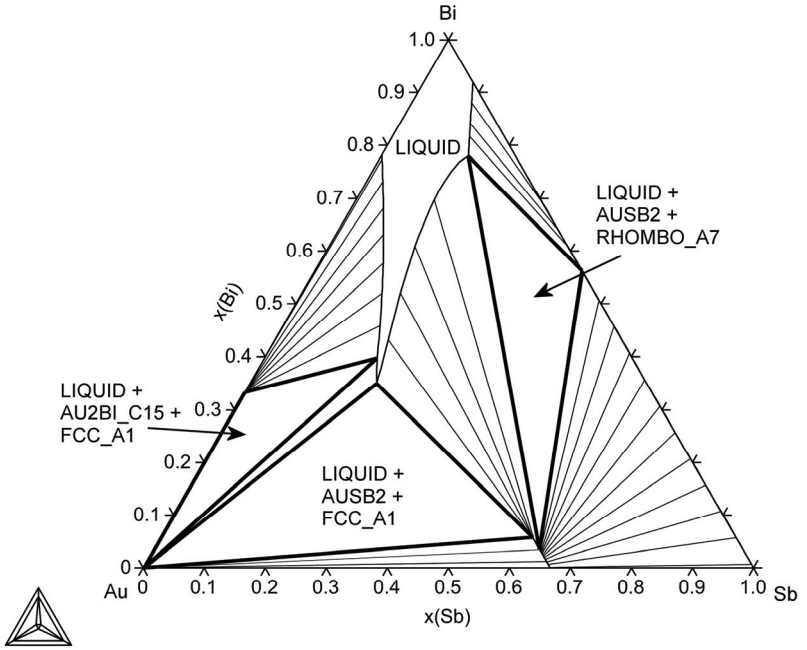

Fig. 135: Isothermal section at 300 °C

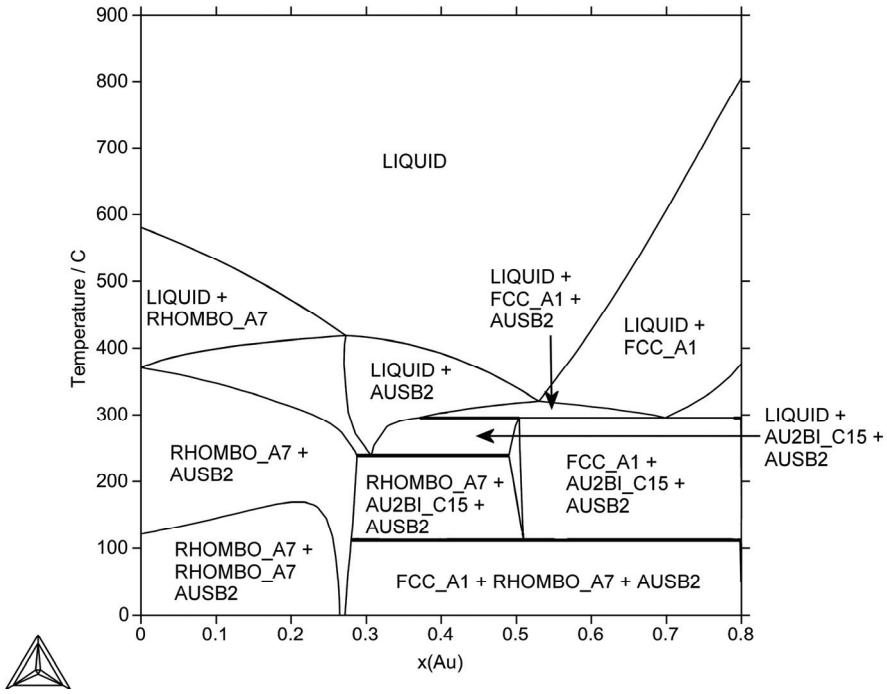

Fig. 136: Isopleth of the Au-Bi-Sb system for 20 at% Bi

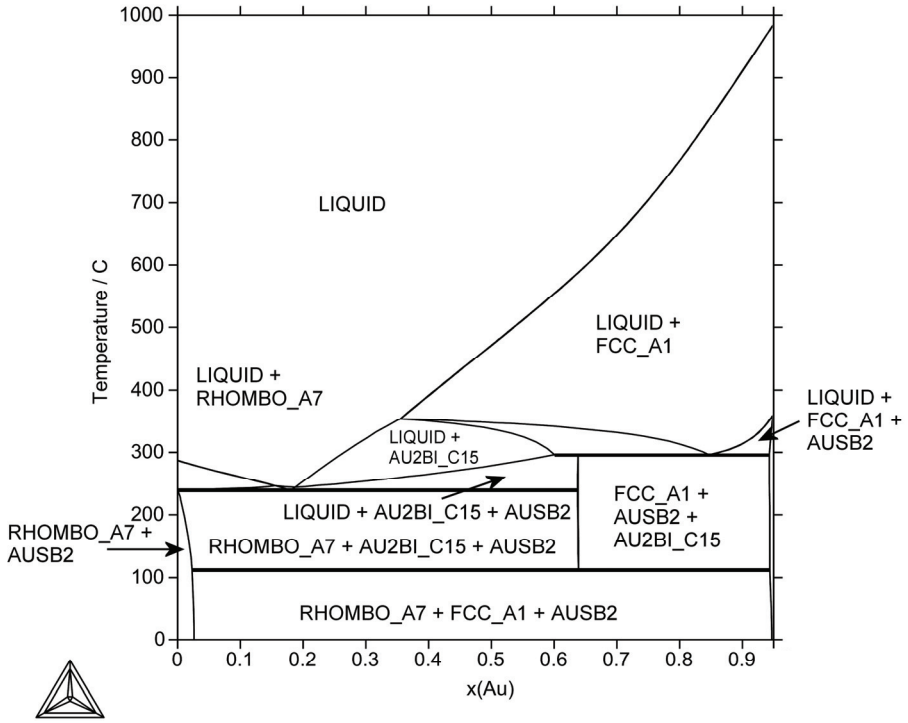

Fig. 137: Isopleth of the Au-Bi-Sb system for 5.2 at% Sb (close to the eutectic point E1)

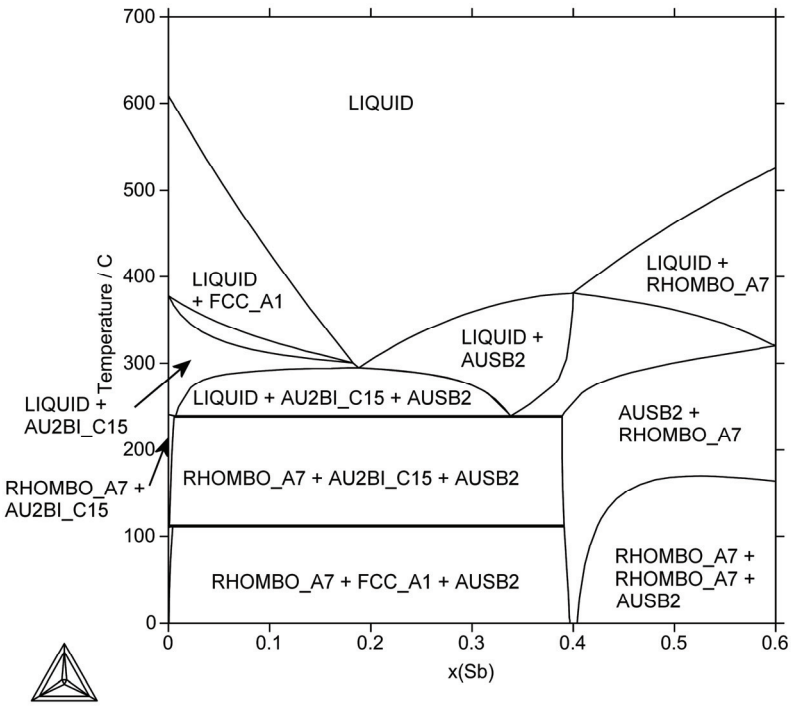

Fig. 138: Isopleth of the Au-Bi-Sb system for 40 at% Bi (close to the univariant point U1)

Au-In-Sb System

Data from the critical assessment of Liu *et al.* **[03Liu]** were adopted after modification in the scope of COST 531 Action. This system exhibits a very complex liquidus surface, which is shown in detail in the diagrams. In particular the T-x projection gives an excellent overview of the invariant points.

References:

[03Liu] Liu, H. S., Liu, C. L., Wang, C., Ishida, K.: *J. Electron. Mater.*, 2003, **32**, 81-88.

Table of invariant reactions

T / °C	Reaction type	Phases	Compositions		
			x_{Au}	x_{In}	x_{Sb}
376.5	P1	LIQUID	0.651	0.264	0.085
		AUIN_GAMMA	0.700	0.300	0.000
		AU3IN	0.750	0.250	0.000
		AU7IN3	0.700	0.300	0.000
364.5	U1	LIQUID	0.619	0.299	0.082
		AUIN_GAMMA	0.694	0.306	0.000
		AUIN_PSI	0.630	0.370	0.000
		AU7IN3	0.700	0.300	0.000
349.0	U2	LIQUID	0.376	0.363	0.261
		AUIN2	0.333	0.639	0.028
		ZINCBLENDE_B3	0.000	0.500	0.500
		AUIN	0.500	0.486	0.014
337.4	U3	LIQUID	0.382	0.342	0.276
		ZINCBLENDE_B3	0.000	0.500	0.500
		AUIN	0.500	0.482	0.018
		RHOMBO_A7	0.000	0.001	0.999
334.9	U4	LIQUID	0.651	0.105	0.244
		FCC_A1	0.916	0.081	0.003
		AUSB2	0.333	0.000	0.667
		DHCP	0.895	0.105	0.000

331.5	U5	LIQUID	0.651	0.117	0.232
		DHCP	0.886	0.114	0.000
		AUSB2	0.333	0.000	0.667
		HCP_A3	0.865	0.132	0.003
322.1	U6	LIQUID	0.448	0.296	0.256
		RHOMBO_A7	0.000	0.000	1.000
		AUIN	0.500	0.466	0.034
		AUSB2	0.333	0.002	0.665
306.5	U7	LIQUID	0.636	0.191	0.173
		HCP_A3	0.814	0.184	0.002
		AU3IN	0.750	0.250	0.000
		AUSB2	0.333	0.000	0.667
300.5	E1	LIQUID	0.616	0.222	0.162
		AU7IN3	0.700	0.300	0.000
		AU3IN	0.750	0.250	0.000
		AUSB2	0.333	0.000	0.667
293.3	U8	LIQUID	0.565	0.274	0.161
		AUIN	0.500	0.454	0.046
		AUSB2	0.333	0.001	0.666
		AUIN_PSI	0.616	0.384	0.000
291.8	E2	LIQUID	0.574	0.269	0.157
		AUSB2	0.333	0.001	0.666
		AUIN_PSI	0.619	0.381	0.000
		AU7IN3	0.700	0.300	0.000
154.4	E3	LIQUID	0.001	0.995	0.004
		AUIN2	0.333	0.6667	0.000
		ZINCBLENDE_B3	0.000	0.500	0.500
		TETRAG_A6	0.000	1.000	0.000

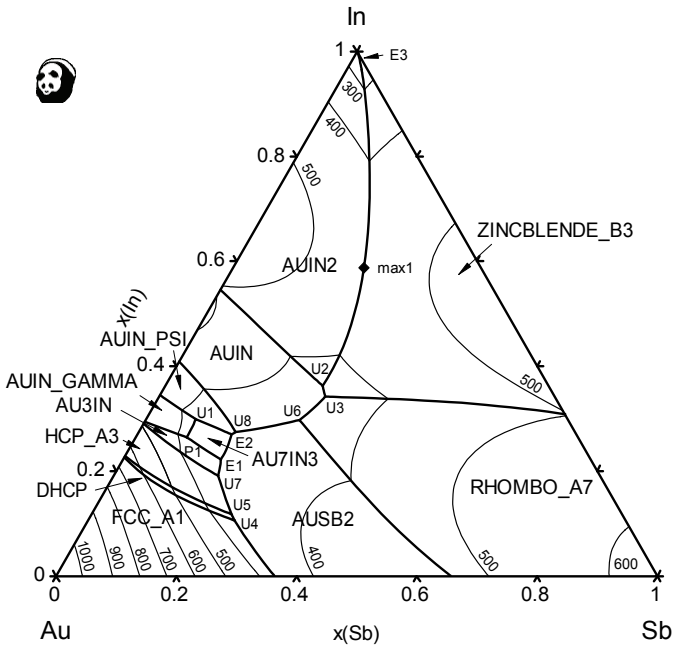

Fig. 139: Liquidus surface of the Au-In-Sb system

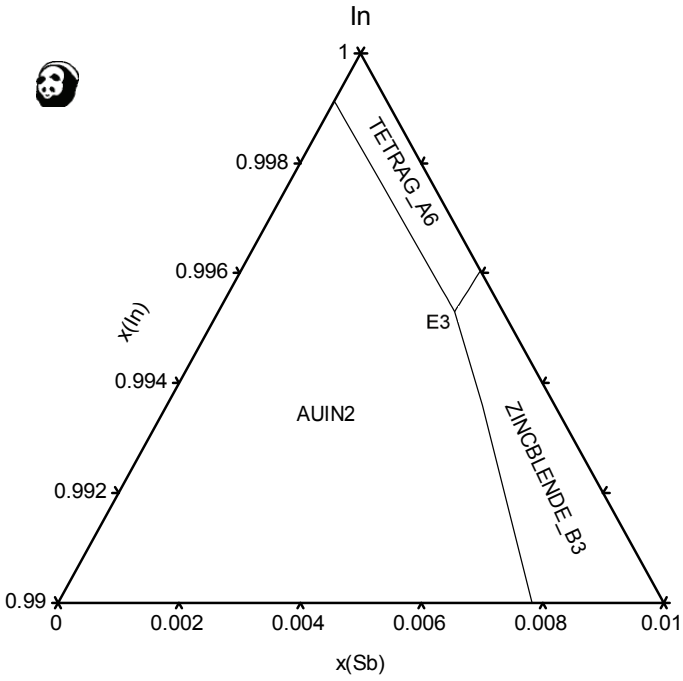

Fig. 140: Magnified view of the In -rich corner of the liquidus surface of the Au-In-Sb system

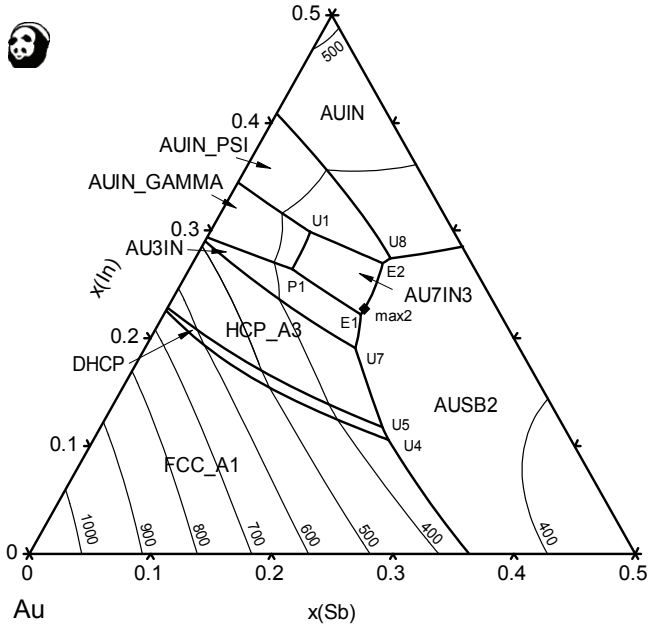

Fig. 141: Magnified view of the Au-rich corner of the liquidus surface of the Au-In-Sb system

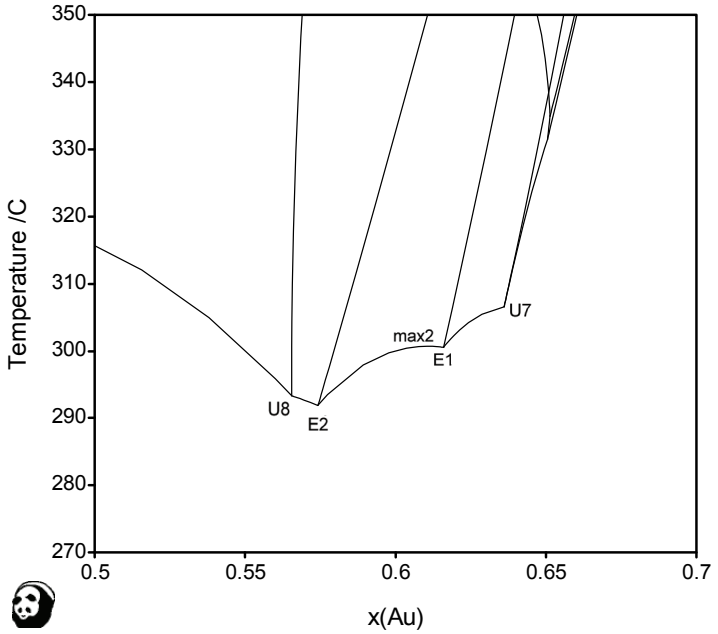

Fig. 142: Liquidus lines in the Au-In-Sb system in the region of the low temperature invariants projected onto the T- x(Au) plane

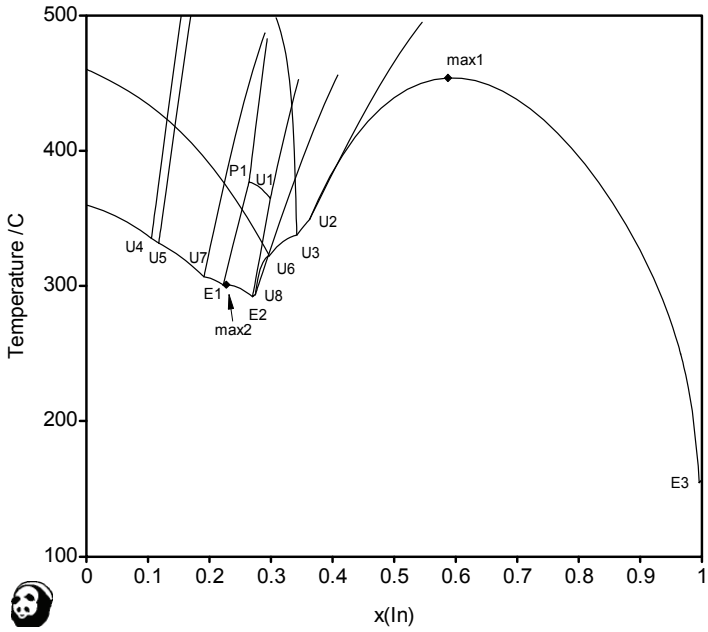

Fig. 143: Liquidus lines in the Au-In-Sb system in the region of the low-temperature invariants projected onto the T- x(In) plane

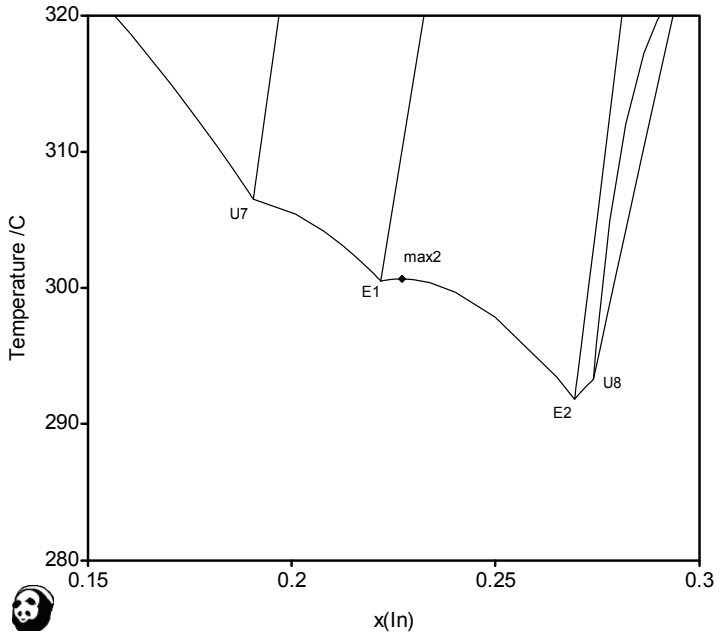

Fig. 144: Detail of liquidus lines in the Au-In-Sb system in the region of the low-temperature invariants projected onto the T- x(In) plane

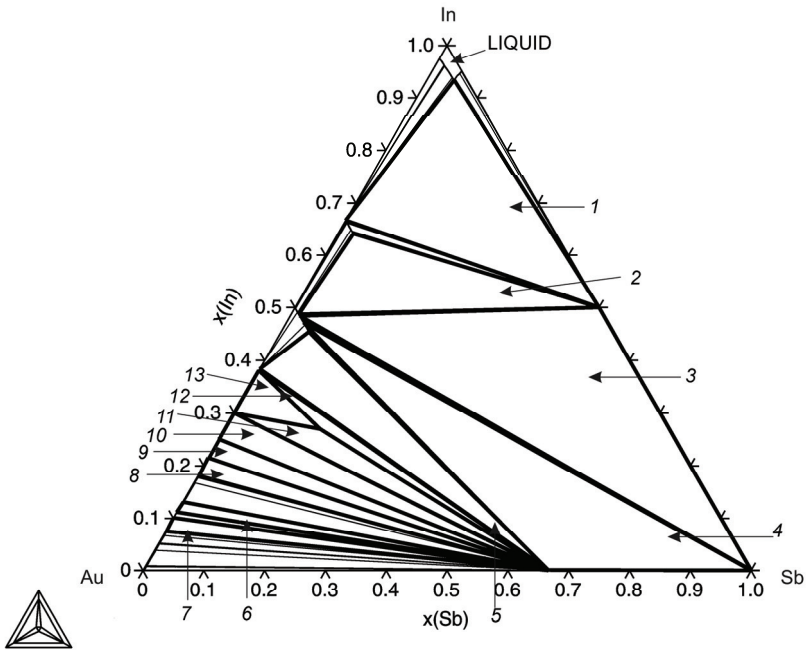

Fig. 145: Isothermal section at 292 °C

Legend:

1 – LIQUID + AUIN2 + ZINCBLENDE_B3
2 – AUIN2 + AUIN + ZINCBLENDE_B3
3 – AUIN + RHOMBO_A7 + ZINCBLENDE_B3
4 – AUIN + AUSB2 + RHOMBO_A7
5 – AUIN + AUSB2 + AUIN_PSI
6 – DHCP + AUSB2 + HCP_A3
7 – DHCP + AUSB2 + FCC_A1
8 – AUIN_ETAP + AUSB2 + HCP_A3
9 – AU3IN + AUIN_ETAP + AUSB2
10 – AU3IN + AU7IN3 + AUSB2
11 – LIQUID + AU7IN3 + AUSB2
12 – LIQUID + AUSB2 + AUIN_PSI
13 – LIQUID + AU7IN3 + AUIN_PSI

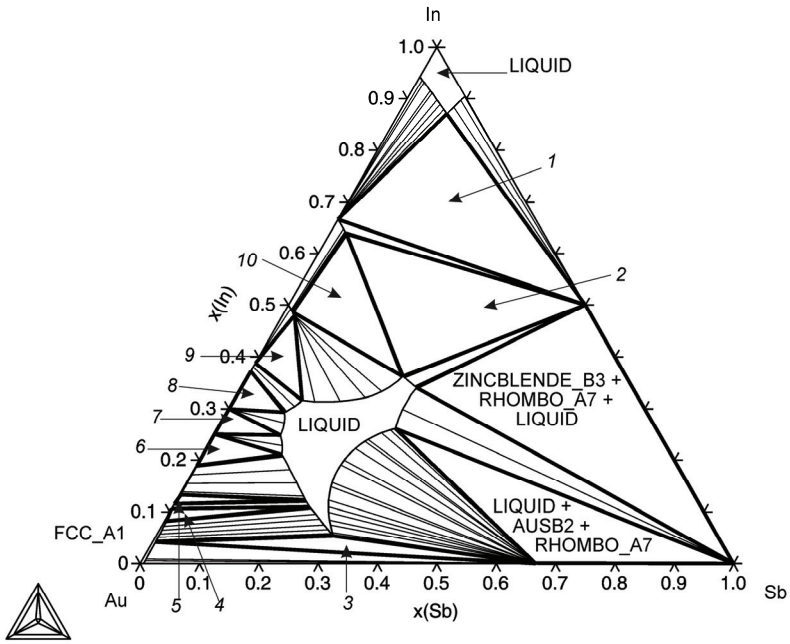

Fig. 146: Isothermal section at 350 °C

Legend:

1 – LIQUID + AUIN2 + ZINCBLENDE_B3
2 – LIQUID + AUIN2 + ZINCBLENDE_B3
3 – LIQUID + AUSB2 + FCC_A1
4 – LIQUID + DHCP + FCC_A1
5 – LIQUID + DHCP + HCP_A3
6 – LIQUID + AU3IN + HCP_A3
7 – LIQUID + AU3IN + AU7IN3
8 – LIQUID + AU7IN3 + AUIN_PSI
9 – LIQUID + AUIN + AUIN_PSI
10 – LIQUID + AUIN + AUIN2

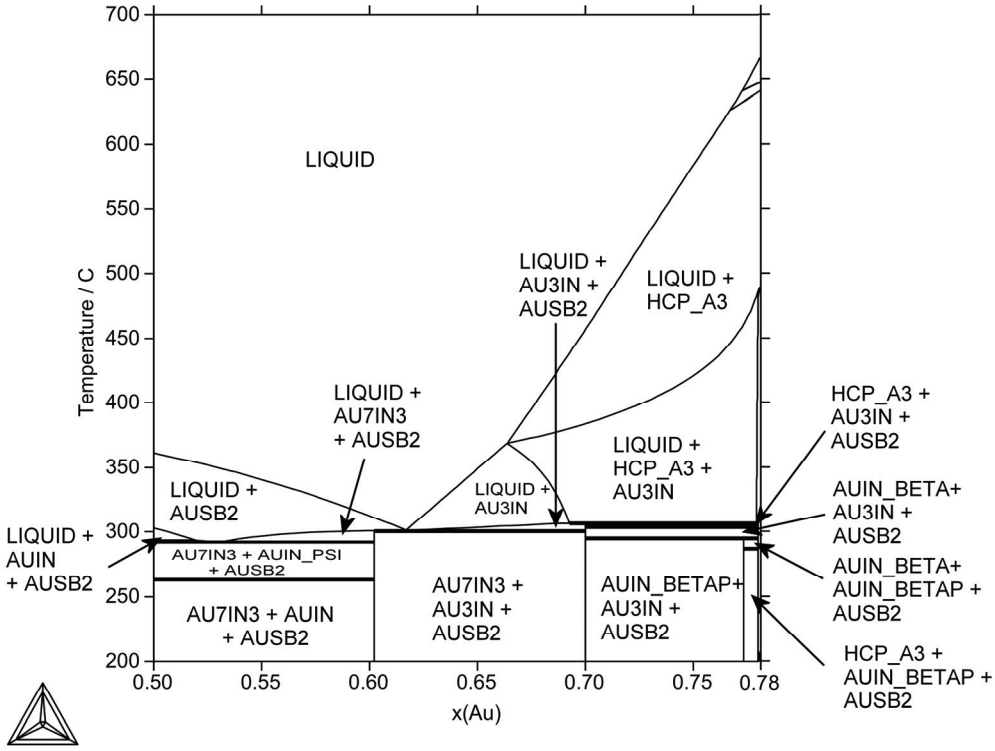

Fig. 147: Part of the isopleths of the Au-In-Sb system for 22 at% In (close to the E1 eutectic point)

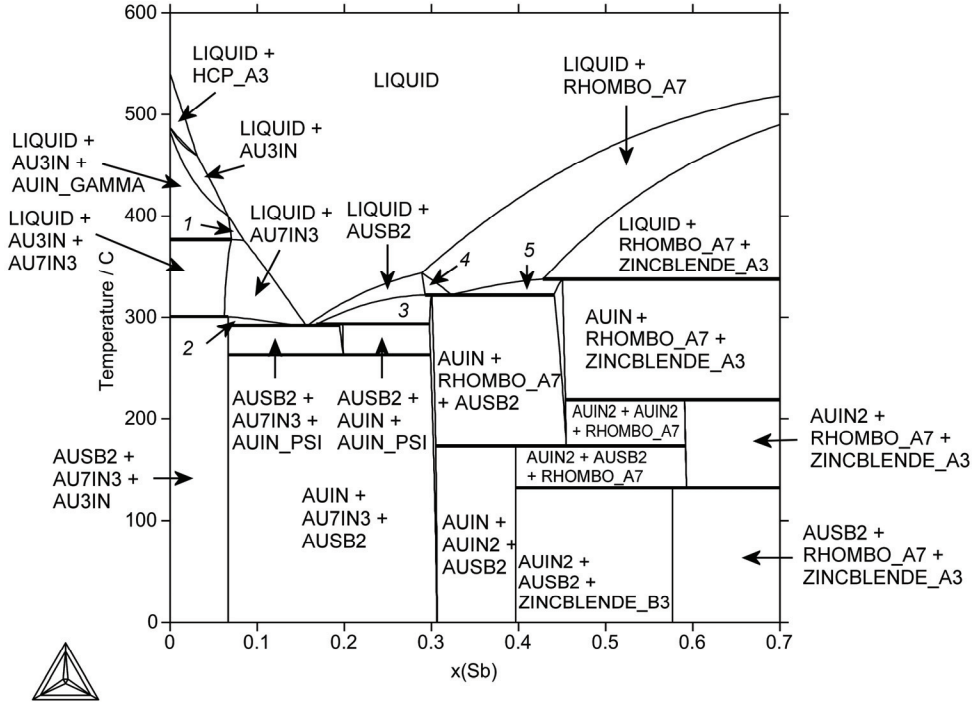

Fig. 148: Isopleth of the Au-In-Sb system for 27 at% In (close to the E2 eutectic point)

Legend:

1 – LIQUID + AUIN_GAMMA
2 – LIQUID + AU7IN3 + AUSB2
3 – LIQUID + AUIN + AUSB2
4 – LIQUID +AUSB2 + RHOMBO_A7
5 – LIQUID + AUIN + RHOMBO_A7

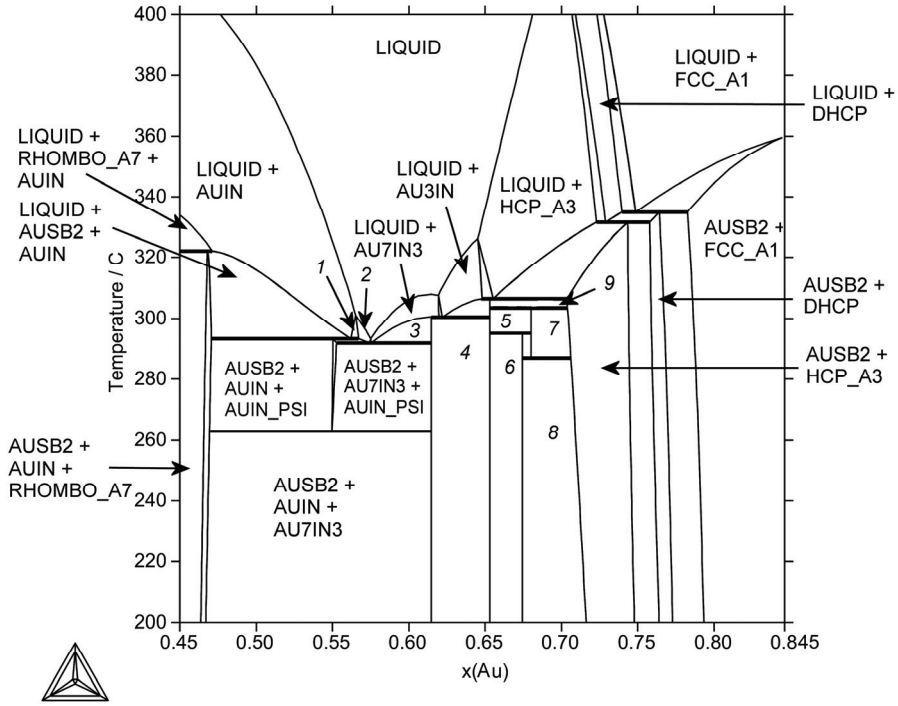

Fig. 149: Partial isopleth of the Au-In-Sb system for 15.5 at% Sb (close to the E2 eutectic point)

Legend:

1 – LIQUID + AUIN + AUIN_PSI
2 – LIQUID + AUIM_PSI
3 – LIQUID + AU7IN3 + AUSB2
4 – AUIN3 +AU7IN3 + AUSB2
5 – AUIN3 + AUIN_BETA + AUSB2
6 – AUIN3 + AUIN_BETAP + AUSB2
7 – AUIN_BETA + AUSB2 + HCP_A3
8 – AUIN_BETAP+ AUSB2 + HCP_A3
9 – AU3IN + AUSB2 + HCP_A3

Au-In-Sn System

This system had not been assessed prior to COST 531. Phase diagram data for the system are sparse. Therefore, a full experimental determination of the system was undertaken under the Action comprising a series of phase diagram studies to confirm previous observations of the phase relationships, DTA and DSC studies to fully characterise the melting behaviour of the ternary AU4IN3SN3 compound, determination of the enthalpy of formation of the ternary compound by direct and tin-solution calorimetry and measurement of the enthalpies of mixing of liquid alloys. The experimental results were used in a CALPHAD assessment of the system, which will be published, along with the experimental data in a series of publications to be submitted to the CALPHAD journal **[08Bor, 08Wat, 08Cac]**.

The ternary compound was found to melt incongruently, contradicting earlier work. The liquidus surface is deceptively complex, as can be realised from the T-x(In) projection, partly owing to primary solidification surfaces for AU7IN3 and the ternary compound in the ternary system. There are 11 transition reactions, two ternary peritectic reactions and 2 ternary eutectics. The transition reaction U5 is more like a catatectic reaction in that the liquid phase is a product of the invariant reaction rather than a reactant. **Fig. 150** shows the whole liquidus surface. The invariant U1 is very close to the In-axis, and associated with it is a very small AU3IN primary surface that is barely visible in the diagram. Likewise reactions U11 and E2 are very close to the Sn-axis, and these are shown in **Fig. 151**, which is a magnification of the region at low Au-contents. The T-x(In) projection (**Fig. 152**) is exceedingly complex, particularly in the 200-500 °C temperature range, and this part of the projection has been magnified in **Fig. 153**. The transition reaction, U5, has the appearance of a ternary peritectic, but this is due to catatectic nature, the liquid phase being a precipitating rather than a reactant phase. From the magnified liquidus surface (**Fig. 151**) and the full T-x(In) projection (**Fig. 152**) it can be seen that the lowest temperature at which liquid is stable is at the ternary eutectic, E2, very close to the In-Sn binary edge. Four maxima appear on the liquidus lines; two at high temperatures associated with the peritectic formation of the DHCP and HCP_A3 phases, and two at lower temperatures; between U2 and U4, and between E1 and E2, very close to E1 and at a temperature of only .01 °C higher. The closeness of the temperature of this maximum and that of E1 would suggest that the nature of the ternary invariant is actually degenerate.

The enthalpies of mixing of liquid alloys were determined at 600 °C along sections of constant In/Sn ratio of 1/1, 1/3 and 3/1 by high-temperature drop calorimetry **[08Wat]**. **Fig. 154** shows calculated enthalpy of mixing curves compared with the experimental values and the level of agreement is very good.

Figs. 155 and **156** show calculated isothermal sections for 130 and 250 °C, respectively. Many of the equilibria at medium to low-In contents were verified experimentally as part of the COST 531 Action; however the equilibria at Au-contents of less than 80 at% are unknown. It's worth noting that the AUIN and AU1SN compounds do not form a continuous series of solid solutions, despite there being a certain degree of mutual solid solubility, but there is a two-phase equilibrium between them. **Figs. 157** and **158** show isopleths for the sections x(Au)-x(In)=0.1 and x(Sn)-2/3x(In)=0.1, together with experimental data from **[08Bor]**.

References:

[08Bor] Borzone, G., Cacciamani, G., Watson, A.: to be submitted to *CALPHAD*, 2008.

[08Wat] Watson, A., Borzone, G., Cacciamani, G.: to be submitted to *CALPHAD*, 2008.

[08Cac] Cacciamani, G., Watson, A., Borzone, G.: to be submitted to *CALPHAD*, 2008.

Table of invariant reactions

T / °C	Reaction type	Phases	Compositions		
			x_{Au}	x_{In}	x_{Sn}
471.6	U1	LIQUID	0.704	0.286	0.010
		AUIN	0.750	0.250	0.000
		AUIN_GAMMA	0.708	0.292	0.000
		HCP_A3	0.786	0.205	0.009
433.8	U2	LIQUID	0.378	0.263	0.359
		AUIN	0.500	0.372	0.128
		AU1SN	0.500	0.202	0.298
		AUIN2	0.333	0.546	0.121
392.0	U3	LIQUID	0.647	0.265	0.088
		AUIN_PSI	0.632	0.368	0.000
		AUIN	0.500	0.380	0.120
		AUIN_GAMMA	0.695	0.305	0.000

384.4	U4	LIQUID	0.650	0.236	0.114
		AUIN	0.500	0.369	0.131
		AU1SN	0.500	0.196	0.304
		AUIN_GAMMA	0.695	0.305	0.000
383.6	P1	LIQUID	0.319	0.151	0.530
		AU1SN	0.500	0.148	0.352
		AUIN2	0.333	0.498	0.169
		AU4IN3SN3	0.400	0.271	0.329
376.5	U5	AUIN_GAMMA	0.699	0.301	0.000
		HCP_A3	0.776	0.180	0.044
		LIQUID	0.679	0.141	0.180
		AU7IN3	0.700	0.300	0.000
373.1	U6	LIQUID	0.662	0.168	0.171
		AUIN_GAMMA	0.696	0.304	0.000
		AU1SN	0.500	0.178	0.322
		AU7IN3	0.700	0.300	0.000
351.2	U7	LIQUID	0.676	0.093	0.231
		AU7IN3	0.700	0.300	0.000
		HCP_A3	0.780	0.171	0.049
		AU1SN	0.500	0.156	0.344
301.4	U8	LIQUID	0.253	0.032	0.715
		AU1SN	0.500	0.059	0.441
		AU4IN3SN3	0.400	0.215	0.385
		AUSN2	0.333	0.000	0.667
267.0	P2	LIQUID	0.161	0.048	0.791
		AU4IN3SN3	0.400	0.252	0.348
		AUSN2	0.333	0.000	0.667
		AUSN4	0.200	0.066	0.734

265.1	U9	LIQUID	0.144	0.065	0.791
		AU4IN3SN3	0.400	0.265	0.335
		AUIN2	0.333	0.447	0.220
		AUSN4	0.200	0.089	0.711
208.0	U10	LIQUID	0.037	0.075	0.888
		AUSN4	0.200	0.133	0.667
		AUIN2	0.333	0.510	0.156
		BCT_A5	0.000	0.020	0.980
207.8	E1	LIQUID	0.033	0.085	0.882
		AUIN2	0.333	0.522	0.145
		INSN_GAMMA	0.000	0.042	0.958
		BCT_A5	0.000	0.024	0.976
140.2	U11	LIQUID	0.001	0.853	0.146
		TETRAG_A6	0.000	0.876	0.124
		AUIN2	0.333	0.664	0.003
		TET_ALPHA1	0.000	0.868	0.132
117.5	E2	LIQUID	0.001	0.525	0.474
		AUIN2	0.333	0.650	0.016
		INSN_GAMMA	0.000	0.227	0.773
		TET_ALPHA1	0.000	0.555	0.445

Phase information

Phase Name	Common Name	Strukturbericht designation/type	Pearson Symbol
AU4IN3SN3	$Au_4In_3Sn_3$	…	…

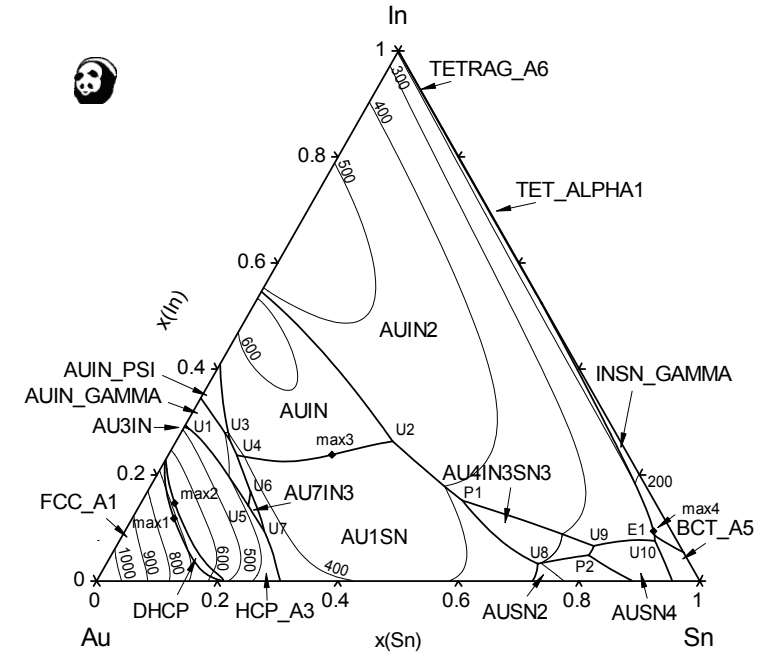

Fig. 150: Liquidus projection of the Au-In-Sn system

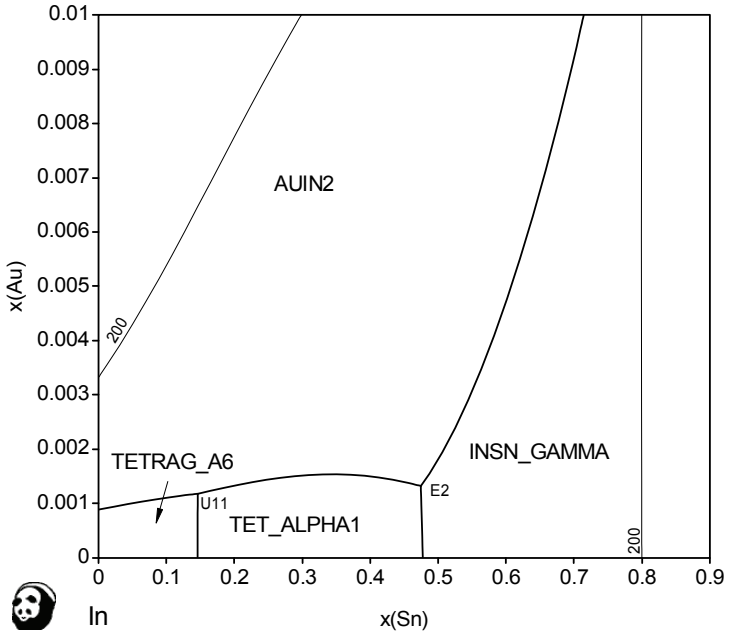

Fig. 151: Liquidus surface of the Au-In-Sn system at low Au-contents

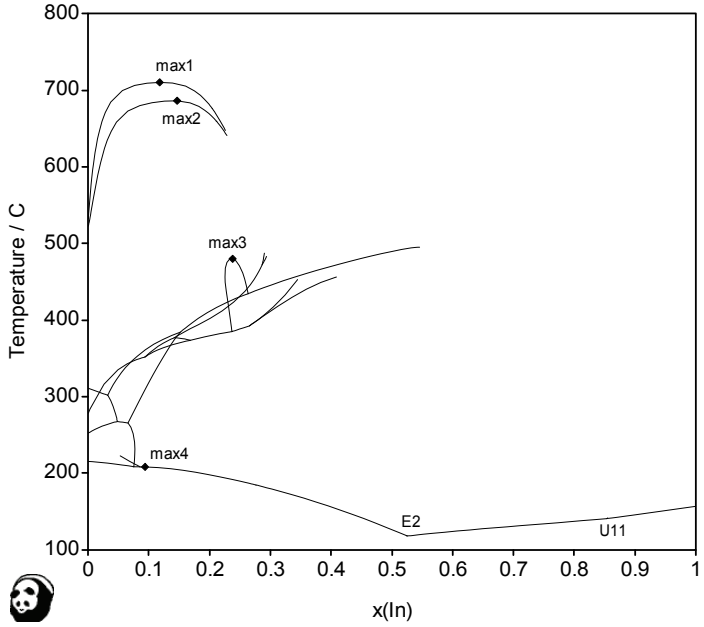

Fig. 152: Liquidus lines in the Au-In-Sn system projected onto the T-x(In) plane

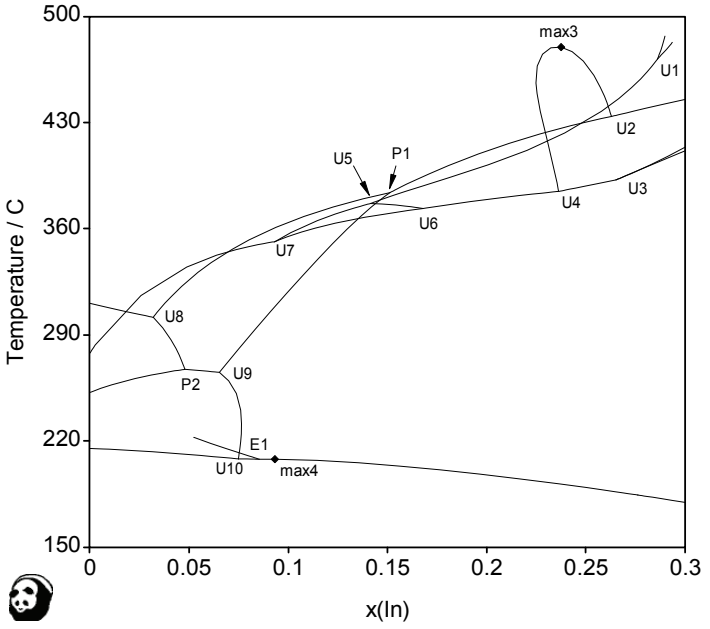

Fig. 153: Liquidus lines in the Au-In-Sn system in the region of the low-temperature invariants projected onto the T- x(In) plane

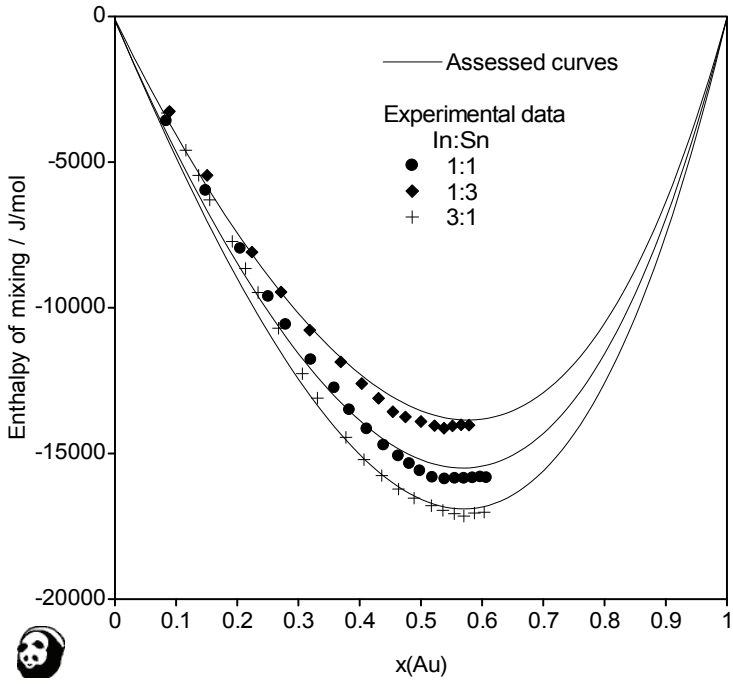

Fig 154: Calculated enthalpies of mixing for liquid alloys at 600 °C, compared with experimental data. Ref. state: Liquid alloy

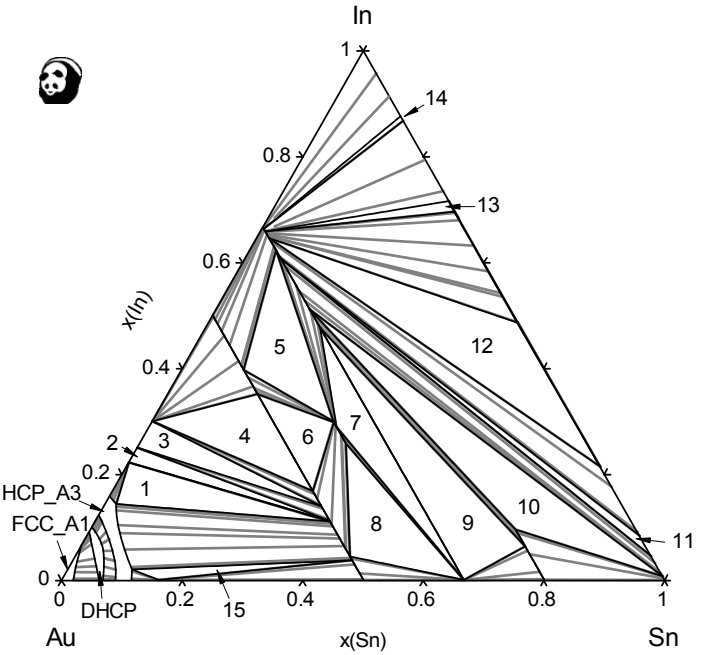

Fig. 155: Isothermal section at 130 °C

Legend:

1 - HCP_A3+AU1SN+AUIN_BETAP
2 - AU1SN+AU3IN+AUIN_BETAP
3 - AU7IN3+AU1SN+AU3IN
4 - AU7IN3+AUIN+AU1SN
5 - AU4IN3SN3+AUIN+AUIN2
6 - AU4IN3SN3+AUIN+AU1SN
7 - AUSN2+AUIN2+AU4IN3SN3
8 - AUSN2+AU4IN3SN3+AU1SN
9 - AUSN2+AUIN2+AUSN4
10 - AUIN2+BCT_A5+AUSN4
11 - AUIN2+BCT_A5+INSN_GAMMA
12 - LIQUID+AUIN2+INSN_GAMMA
13 - LIQUID+AUIN2+TET_ALPHA1
14 - AUIN2+TETRAG_A6+TET_ALPHA1
15 - HCP_A3+AU1SN+AU5SN

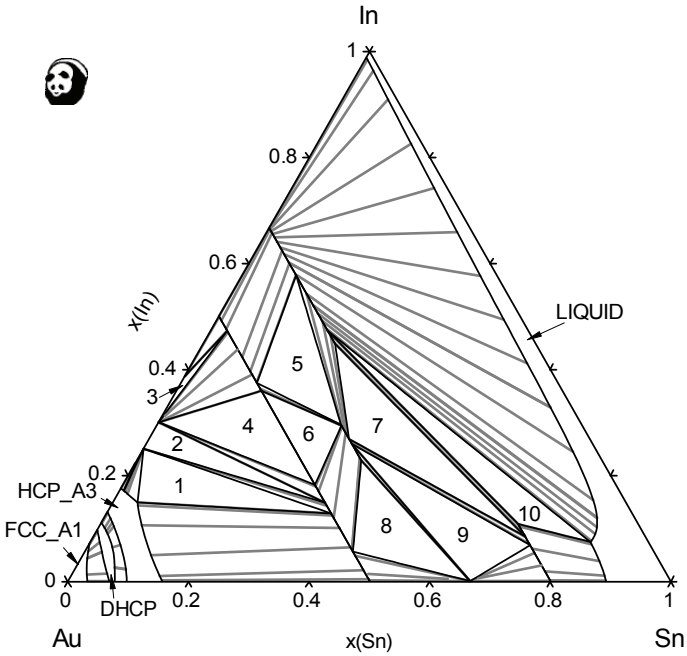

Fig. 156: Isothermal section at 250 °C

Legend:
1 - HCP_A3+AU1SN+AU3IN
2 - AU7IN3+AU1SN+AU3IN
3 - AU7IN3+AUIN+AUIN_PSI
4 - AU7IN3+AUIN+AU1SN
5 - AUIN2+AUIN+AU4IN3SN3
6 - AU4IN3SN3+AU1SN+AUIN
7 - AUIN2+AU4IN3SN3+AUSN4
8 - AUSN2+AU4IN3SN3+AU1SN
9 - AU4IN3SN3+AUSN2+AUSN4
10 - LIQUID+AUIN2+AUSN4

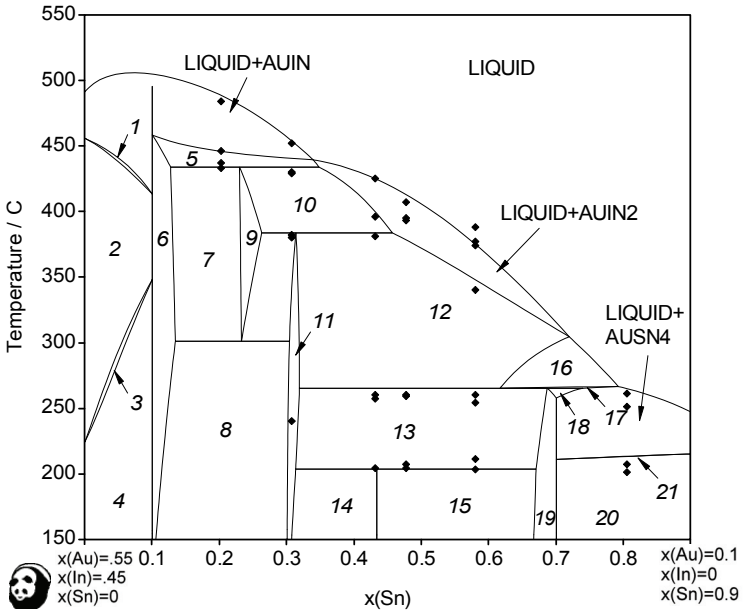

Fig. 157: Isopleth of the Au-In-Sn system x(Au)-x(In)=0.1

Legend:

1 – LIQUID+AUIN+AUIN_PSI
2 – AUIN+AUIN+PSI
3 – AU7IN3+AUIN_PSI+AUIN
4 – AU7IN3+AUIN
5 – LIQUID+AUIN+AUIN2
6 – AUIN+AUIN2
7 – AUIN+AUIN2+AU1SN
8 – AUIN+AUIN2+AU4IN3SN3
9 – AUIN2+AU1SN
10 – LIQUID+AUIN2+AU1SN
11 – AU4IN3SN3+AUIN2
12 – LIQUID+AUIN2+AU4IN3SN3
13 – AUIN2+AUSN4+AU4IN3SN3
14 – AUSN2+AUIN2+AU4IN3SN3
15 – AUIN2+AUSN2+AUSN4
16 – LIQUID+AU4IN3SN3
17 – LIQUID+AU4IN3SN3+AUSN4
18 – LIQUID+AUIN2+AUSN4
19 – AUSN4+AUIN2
20 – AUSN4+BCT_A5
21 – LIQUID+AUSN4+BCT_A5

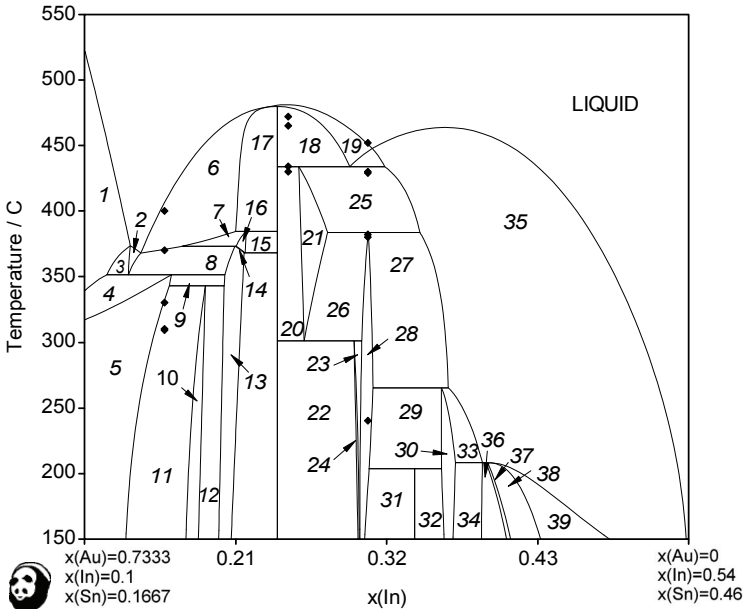

Fig. 158: Isopleth of the Au-In-Sn system at x(Sn)-2/3x(In)=0.1

Legend

1 – LIQUID+HCP_A3
2 – LIQUID+AU7IN3
3 – LIQUID+HCP_A3+AU7IN3
4 – LIQUID+HCP_A3+AU1SN
5 – AU1SN+HCP_A3
6 – LIQUID+AU1SN
7 - LIQUID+AU1SN+AUIN_GAMMA
8 – LIQUID+AU1SN+AU7IN3
9 – AU1SN+AU7IN3+HCP_A3
10 – AU1SN+AU3IN
11 – AU3IN+AU1SN+HCP_A3
12 – AU3IN+AU7IN3+AU1SN
13 – AU7IN3+AU1SN
14 – AU1SN+AUIN_GAMMA+AU7IN3
15 – AUIN+AU1SN+AUIN_GAMMA
16 – AU1SN+AUIN_GAMMA
17 – LIQUID+AU1SN+AUIN
18 – LIQUID+AUIN+AU1SN
19 – LIQUID+AUIN
20 – AUIN+AUIN2+AU1SN
21 – AU1SN+AUIN2
22 – AU4IN3SN3+AU1SN+AUIN
23 – AUIN+AUIN2+AU4IN3SN3
24 – AU4IN3SN3+AUIN
25 – LIQUID+AUIN2+AU1SN
26 – AU4IN3SN3+AUIN2+AU1SN
27 – LIQUID+AUIN2+AU4IN3SN3
28 – AUIN2+AU4IN3SN3
29 – AUIN2+AU4IN3SN3+AUSN4
30 – AUIN2+AUSN4
31 – AUSN2+AUIN2+AU4IN3SN3
32 – AUIN2+AUSN2+AUSN4
33 – LIQUID+AUIN2+AUSN4
34 – AUIN2+AUSN4+BCT_A5
35 – LIQUID+AUIN2
36 – AUIN2+BCT_A5
37 – AUIN2+BCT_A5+INSN_GAMMA
38 – AUIN2+INSN_GAMMA
39 – LIQUID+AUIN2+INSN_GAMMA